Solving heat conduction problems with a moving heat source in arc welding processes via an overlapping nodes scheme based on the improved element-free Galerkin method

Álvarez Hostos Juan C.,[a,b] Storti Bruno,[a,c] Tourn Benjamín A.[d] and Fachinotti Víctor D.[a]

[a]Centro de Investigación de Métodos Computacionales (CIMEC), Universidad Nacional del Litoral (UNL)/Consejo Nacional de Investigaciones Científicas y Técnicas (CONICET), Predio CCT-CONICET Santa Fe, Argentina

[b]Department of Materials, Faculty of Chemical Engeneering, Universidad Nacional del Litoral (UNL), Santa Fe, Argentina

[c]Université de Nantes, CNRS, Laboratoire de thermique et énergie de Nantes, LTeN, UMR 6607, F-44000 Nantes, France

[d]Centro de Investigación y Transferencia (CIT) Rafaela, Universidad Nacional de Rafaela (UNRaf)/Consejo Nacional de Investigación Científicas y Técnicas (CONICET)

Abstract

A novel overlapping nodes scheme developed in the framework of an improved element-free Galerkin (IEFG) formulation is introduced in order to solve the transient heat conduction problem with a moving heat source involved in arc welding processes, in an accurate and remarkably simple manner. The proposed approach consists in solving the aforementioned problem over two overlapping arrangements of nodes, which transfer temperature and heat flux information each other through properly defined immersed boundaries. A fine arragement of nodes (patch nodes) moves with the heat source over a coarse background nodes distribution, and the solution is enriched via an appropriate coupling of the temperature approximations computed over both arrangements. The patch nodes are conceived to achieve an accurate computation of the temperature distribution and corresponding heat fluxes in the heat source vicinity, whose effects cannot be properly captured by the coarse background arrangement. A detailed explanation concerning the appropriate coupling between the temperature fields of both the background and patch nodes, is also provided in this communication. The outcomes of this study reveal that the proposed Overset-IEFG (Ov-IEFG) formulation allows the achievement of very accurate, smooth and stable solutions for both temperature and heat flux fields, without the need of resorting to post-processing or additional local reconstruction techniques.

Keywords: Transient heat conduction, Arc welding, Moving Heat Source, Element-free Galerkin method, Penalty, Overlapping Nodes

Nomenclature

Transient heat conduction problem

T	Temperature
ρ	Density
c_p	Specific heat capacity
k	Conductivity
$\dot{Q}$	Heat source

Ov-IEFG Formulation

$\mathbf{C}^{\mathrm{BG}}$ / C_{IJ}^{BG}	Capacitance Matrix for Background Nodes/Single Component
$\mathbf{K}^{\mathrm{BG}}$ / K_{IJ}^{BG}	Conductivity Matrix for Background Nodes/Single Component
$\mathbf{P}^{\mathrm{BG}}$ / P_{IJ}^{BG}	Essential Conditions Penalty Matrix for Background Nodes/Single Component
$\mathbf{C}^{\mathrm{PC}}$ / C_{IJ}^{PC}	Capacitance Matrix for Patch Nodes/Single Component
$\mathbf{K}^{\mathrm{PC}}$ / K_{IJ}^{PC}	Conductivity Matrix for Patch Nodes/Single Component
$\mathbf{A}^{\mathrm{PC}}$ / A_{IJ}^{PC}	Advective Transport Matrix for Patch Nodes/Single Component
$\mathbf{P}^{\mathrm{PC}}$ / P_{IJ}^{PC}	Conditions Penalty Matrix for Patch Nodes/Single Component
$\mathbf{F}^{\mathrm{BG}(\dot{Q})}$ / $F_I^{\mathrm{BG}(\dot{Q})}$	Heat Source Loads Vector for Background Nodes/Single Component
$\mathbf{F}^{\mathrm{BG}(\bar{q})}$ / $F_I^{\mathrm{BG}(\bar{q})}$	Surface Heat Flux loads Vector for Background Nodes/Single Component
$\mathbf{F}^{\mathrm{BG}(h_p)}$ / $F_I^{\mathrm{BG}(h_p)}$	Essential Conditions Loads Vector for Background Nodes/Single Component
$\mathbf{F}^{\mathrm{PC}(\dot{Q})}$ / $F_I^{\mathrm{PC}(\dot{Q})}$	Heat Source Loads Vector for Patch Nodes/Single Component
$\mathbf{F}^{\mathrm{PC}(h_p)}$ / $F_I^{\mathrm{PC}(h_p)}$	Essential Conditions Loads Vector for Patch Nodes/Single Component

1. Introduction

The appropriate joining of structural elements via arc welding demands an accurate control of the transient heat transfer phenomena involved in such a manufacturing process, which has a crucial effect in the mechanical properties of the welded parts and quality of the joint. These features reveal the significance of developing techniques, whether theoretical or numerical, conceived to solve heat transfer problems concerning arc welding as accurately as possible. In this sense, several researchers have devoted special efforts to achieve accurate solutions for heat transfer problems involved in arc welding processes, via analytical, semi-analytical, and numerical approaches. Some of

*Corresponding author: Álvarez Hostos J. C. Currently postdoctoral fellow at: Computational Methods Research Centre, National Scientific and Technical Research Council, Argentina. Contact email: jchostos@cimec.unl.edu.ar

the solutions achieved via analytical and semi-analytical approaches include: The transient heat conduction problems solved by Nguyen et al. concerning double ellipsoidal heat sources in uniform rectilinear motion in both semi-infinite bodies [1] and finite thick plates [2], the solutions developed by Winczek [3] for moving heat sources describing arbitrary paths in semi-infinite bodies, the improvement introduced by Fachinotti et al. [4] for the appropriate integration of double ellipsoidal moving heat sources, the semi-analytical model for two-dimensional transient heat conduction problems with moving heat sources developed by Veldman et al. [5] via a splitting approach in which the problem in two spatial dimensions is decoupled in three one-dimensional problems, and the semi-analytical model developed by Flint et al. [6] for moving heat sources in three-dimensional finite orthogonal domains. The heat transfer in arc welding is modelled via the solution of a transient heat conduction problem with a variable moving heat source whose power density exhibits a Gaussian distribution in a small circular [7], semi-spherical [1], single [1] and double [4] semi-ellipsoidal, or conical [6,8] region. On the other hand, numerical methods have allowed the solution of arc welding problems involving several difficulties and non-linearities which, in principle, cannot be addressed via the analytical approach. Such difficulties include the implementation of split or composite heat sources in irregular geometries [8], temperature-dependent properties and phase-change effects [9,10], coupled heat and mass transfer between dissimilar welded materials [11], and non-linear thermo-mechanical analysis including inelastic strains effects [9,10]. The finite element method is a thoroughly developed mesh-based numerical technique, which has been widely and successfully used in the solution of transport phenomena and thermo-mechanical problems inherent in arc welding processes. The achievement of accurate results in the FEM-based numerical solution of transient heat conduction problems in arc welding usually requires a significant mesh refinement along the moving heat source path [4,9] or the implementation of adaptive remeshing procedures [12,13], for an appropriate capture of the corresponding marked thermal gradients. Such a requirement arises from the fact that FEM-based solutions usually involve a piecewise approximation of the field variables, which introduces difficulties to capture high thermal gradients due to the discontinuous derivatives at the elements faces [14]. Such features also make difficult the solution of problems involving moving boundaries, large deformations and material discontinuities that commonly do not coincide with the element or cell boundaries [14]. A feasible alternative conceived to overcome the aforementioned difficulties regarding the FEM and other mesh-based discretization techniques has been found in the implementation of more recently developed meshless or meshfree techniques, whose potential in the solution of increasingly complex heat transfer problems has already been demonstrated by several researchers. Some of these problems include transient heat conduction in both isotropic [15,16] and anisotropic media [17,18], inverse [19] and backwards [20] heat conduction analysis, natural [21,22] and forced [23,24] convection, coupled fluid flow and heat transfer in deformable porous media [25] phase-change in both benchmark [23] an applied [26,27] cases, moving boundaries [28,29], radiative heat transport [30,31], and even topology optimization [32].

The solution of transient heat conduction problems with local moving heat sources are of principal interest in this work, and the studies available in the revised literature concerning the solution of this problem via meshless techniques demonstrate the potential of such approaches to achieve smooth, accurate and stable results in the heated region. The positive features of meshless techniques in the solution of transient heat conduction problems with moving heat sources have been demonstrated in simple benchmark cases [7,33], three-dimensional heat transfer modelling with experimental validation [8], markedly concentrated moving heat sources following curve paths in irregular domains [34], and more complex applied situations such as: transient heat conduction analysis in friction stir welding [35] ,thermo-mechanical modelling of arc-welding [36] and additive manufacturing processes [10,37]. Meshless techniques frequently give rise to a straightforward computation of continuous and smooth distributions in the field variables and the corresponding derivatives, whereby such methods provide a better capturing of high thermal gradients and improve the convergence rate in comparison with mesh-based techniques [23,27]. Some of the meshless methods used to predict the performance of welding processes include: the element-free Galerkin (EFG) method [7,8,10], meshless local Petrov-Galerkin (MLPG) method [36], the finite pointset (FPS) method [33], improved symmetric smooth particle hydrodynamics (ISSPH) [35,37], and also the radial point interpolation method (RPIM) [34]. Among the meshless techniques, the EFG method is a weak-formulation based procedure whose reliability has already been demonstrated in the solution of several interesting problems such as: mechanics of inelastic solids under both small [38,39] and finite [40] strains, heat transfer with phase change in fixed [26,27] and variable [28,29] domains, linear [7,8] and non-linear [10] transient heat conduction with moving heat sources, fluid-dynamics [41,42], fluid-structure interaction [43], coupled fluid flow and heat transfer in homogeneous [21,44] and porous media [25], heat transfer in anisotropic media [17,18], and even bio-medical applications [45,46]. The successful implementation of EFG formulations in the solution of increasingly complex problems has recently allowed an extension of its potential to the thermal and thermo-mechanical analysis of arc welding processes, giving rise to an accurate assessment of the moving heat source effects [7,8] and its implications in additive manufacturing processes [10].

According to the studies discussed so far concerning the implementation of meshless techniques in the solution transient heat conduction problems with moving heat sources, such kind of numerical methods allow the achievement of very accurate results with a coarse nodes distribution in comparison with the mesh refinements usually required in mesh-based solutions. Some accurate results have been

achieved even performing uniform nodes distribution to represent the problem domain in the context of element-free Galerkin [7], finite pointset [33] and meshless local Petrov-Galerkin [36] methods, which overcomes the local mesh refinements demanded in the framework of mesh-based techniques. Such a positive numerical feature has been demonstrated for moving heat sources with effective areas of moderate dimensions, where the smooth-higher order approximations inherent in meshless methods are enough to achieve an accurate computation of the high thermal gradients developed near the heat source. This straightforward achievement of accurate results is not feasible for moving heat sources with effective areas of small dimensions, where the need of performing a local nodes or mesh refinement cannot be overcome regardless the implementation of meshless or mesh-based techniques. A recent development conceived to overcome such issue within the framework of meshless methods has been introduced in the work of Khosravifard et al. [34], where the RPIM has been coupled to an adaptive nodes refinement procedure for the solution of transient heat conduction problems with moving point heat sources. Such a technique has also involved the need of introducing a background decomposition method, in order to conform the integration points to the local nodes refinement during the numerical computation and assembling of the matrices and vectors inherent in the RPIM. It is worth mentioning the particular suitability of alternative boundary-type mesh-based and meshless methods for the solution of heat conduction problems with point heat sources, since in such numerical techniques only the domain boundary must be discretized or represented by a set of elements or nodes (no internal elements or nodes are involved in the numerical approximations). The boundary element method (BEM) is a boundary-type mesh-based technique whose potential has already been demonstrated in problems involving not only static [47] and moving [48] point heat sources, but also concentrated along straight [49] and curved [50] lines. Despite such potential of the BEM to solve problems of this kind, this promising numerical technique also has several disadvantages concerning the mathematical complexity of its formulation, the need for a previous knowledge of the fundamental solution of the problem to be solved, its cumbersome programming, and the singular integrals to be solved at the problem boundaries. A powerful alternative tool to overcome the aforementioned drawbacks of the BEM is a boundary-type meshless technique known as the method of fundamental solutions (MFS), in which the temperature distribution (in the context of heat conduction problems) is approximated via a superposition of fundamental solutions linked to heat sources located on a pseudo-boundary outside the problem domain. Although the MFS is also based on a previous knowledge of the fundamental solutions, it is actually an integration-free method with singular points located outside the problem domain. Such features are the main advantages of the MFS, since there is no need to solve singular integrals at the problem boundaries and the computational cost is low. Such noteworthy advantages of the MFS have allowed a very accurate and efficient solution of steady [51] and transient [52] heat conduction and thermo-elastic problems with both fixed concentrated heat sources, whereby its potential has also been recently used in the solution of thermal [53] and thermo-elastic [54] problems with moving point heat sources. It must be remarked that the main advantage of both BEM and MFS in the solution of transient heat conduction problems with moving point heat sources is the possibility of capture appropriately thermal energy delivered to the problem domain without the need of performing cumbersome rearrangements of internal elements or nodes at each time step, and those used to discretize or represent the domain boundaries remain unchanged.

In agreement to the aspects discussed so far concerning the potential of meshless and mesh-reduction techniques for the solution of heat conduction problems with moving heat sources in arc welding processes, the present work is focused on providing a further development in this regard via the introduction of a novel EFG-based procedure for the solution of transient heat conduction problems with moving heat sources of small effective area. The thermal problem will be solved over two overlapping computational domains represented by different nodes distributions with no topological relationship, but transferring information each other through properly defined immersed boundaries. The EFG formulations developed for the thermal problem over each nodes arrangement are coupled via the imposition of Dirichlet conditions at the moving immersed boundaries, which are enforced via the penalty method and updated until convergence is reached at each time step. Such kind of overlapping nodes scheme is unprecedented in the revised literature, and thus also its implementation in the heat transfer modelling of arc welding processes. The approximation of temperature for the procedure proposed in this communication will be conducted via improved moving least squares (IMLS), which actually leads to an improved element-free Galerkin (IEFG) formulation. Such a novel Overset-IEFG (Ov-IEFG) approach is conceived to make use not only of the IMLS positive features concerning the straightforward achievement of smooth-high order approximations in a moving local support domain, but also the possibility of performing a continuous integration of the coupling Dirichlet conditions (CDC) to be imposed along the immersed boundaries. Such a feature allows the achievement of smooth temperature and heat flux distributions in the transition between both arrangements of nodes, without resorting to the complex post-processing or local reconstruction techniques usually required in the nodes-based piecewise transfer of information inherent in overset techniques developed in the context of FEM or finite volume methods (FVM) [55]. A recent development in this regard and a comprehensive review of overset techniques developed in the framework of FEM and FVM can be found in the work of Storti et al. [55], where a high-order adaptive interpolation algorithm has been introduced in order to achieve a smooth coupling between the temperature fields computed in overlapping non-structured meshes while keeping the convergence features of a one-domain standard FEM-based

solution. It is worth mentioning that -up to the authors' knowledge- the implementation of overset techniques has not yet been introduced in the solution of transient heat conduction problems with moving heat sources in arc welding processes, regardless of whether such procedures are developed within the framework of mesh-based or meshless approaches.

According to the aspects mentioned above, the contributions of this study can be summarized as follows:

- An IEFG-based approach conceived to achieve accurate results in the numerical solution of transient heat conductions problems with moving heat sources of small effective area, in a remarkably simple manner. Such a procedure gives rise to a more comprehensive use of the positive features of the IMLS approximations involved in IEFG formulations, in comparison with the studies so far available in the literature concerning the solution of such heat transfer problem via meshless techniques.

- The introduction of an overset technique in the context of an IEFG formulation, which has given rise to an Ov-IEFG approach unprecedented in the revised literature. Such a procedure involves a straightforward transfer of information between overlapping nodes arrangements via IMLS approximations, which allows the achievement of a smooth transition of the numerical solution at the coupling immersed boundaries without the need of resorting to the local reconstruction techniques commonly required in the framework of FEM and FVM.

- A novel technique for the heat transfer modelling of arc welding processes via a meshless representation of the problem domain involving a moving fine nodes arrangement continuously capturing the high thermal gradients developed near the heat source, and reciprocally transfer numerical information with a fixed-coarse background nodes arrangement for the achievement of an enriched-accurate solution.

- A first approach conceived to circumvent the cumbersome adaptive nodes refinement procedures commonly required within the framework of domain-type meshless methods for the achievement of accurate solutions in transient heat conduction problems with moving heat sources of small effective area, which has been particularly developed using the IEFG method.

2. Governing Equations

The transient heat conduction problem in a domain Ω_{BG} with boundaries Γ_{BG} will be solved via an IEFG formulation developed over a meshless representation consisting of two overlapping set of nodes, and the enriched solution is achieved performing a straightforward transfer of information between both arrangements of nodes via the IMLS approximations.

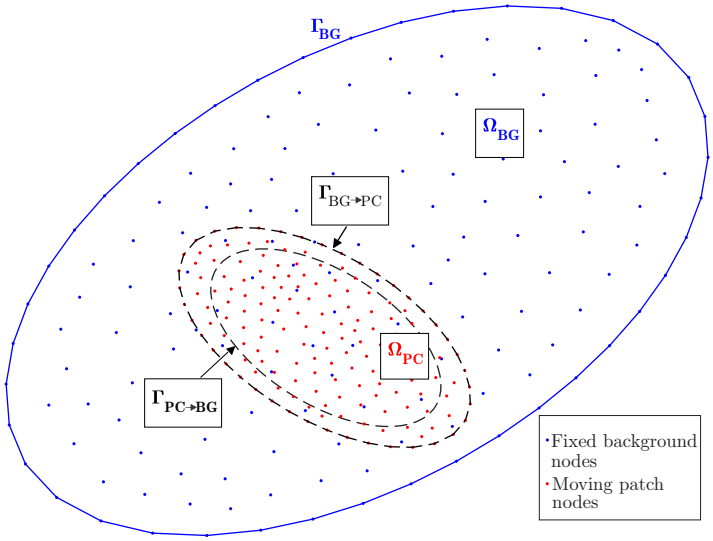

Figure 1: Representation of the problem domain for a numerical solution performed via the Ov-IEFG method.

The proposed methodology is depicted in Fig.1, where a fine distribution of patch nodes (red points) is placed to represent a region Ω_{PC} where thermal gradients are expected to be so high that they cannot be properly captured by the coarse arrangement of background nodes (blue points). The background nodes arrangement is used to perform the numerical solution only in the region $\Omega_{\mathrm{BG}} - \Omega_{\mathrm{PC}}$ of smooth temperature gradients, whereas the patch nodes representing Ω_{PC} are used to achieve an enriched approximation of the temperature distribution in such a region of high numerical accuracy requirements. The transfer of information from Ω_{BG} to Ω_{PC} and visceversa is performed through the immersed boundaries $\Gamma_{\mathrm{BG}\to\mathrm{PC}}$ and $\Gamma_{\mathrm{PC}\to\mathrm{BG}}$, respectively. Such a transfer of information is performed via the imposition of CDC defined from the thermal problem solved over each nodes arrangement, and consequently updated at each time step. The thermal problem solved in Ω_{BG} provides the temperature distribution to be imposed on $\Gamma_{\mathrm{BG}\to\mathrm{PC}}$ (immersed boundary to transfer information from Ω_{BG} to Ω_{PC}), and this information is transferred to Ω_{PC} in the form of a CDC to which the thermal problem to be solved in such moving region is subjected. Similarly, the thermal problem solved in Ω_{PC} provides the temperature distribution to be imposed on $\Gamma_{\mathrm{PC}\to\mathrm{BG}}$ (immersed boundary to transfer information from Ω_{PC} to Ω_{BG}), and this information is the CDC to which the thermal problem to be solved in the fixed background domain Ω_{BG} is subjected. Particularly for the problem to be solved in this study, the region Ω_{PC} represented by the patch nodes constantly moves in order to enclose the heat source at each time step. On the other hand, the coarse arrangement of background nodes is fixed and spans the entire problem domain Ω_{BG}. Such features introduce

some differences in the form of the transient heat conduction equation to be solved over each nodes distribution, and thus in the corresponding IEFG formulations to be properly coupled for the achievement of an enriched numerical solution of the heat transfer problem.

2.1. Transient heat conduction equation for the patch and background node arrangements

The transient heat conduction problem to be solved in the coarse background nodes arrangement concerning the fixed representation of the entire problem domain, is described by the following partial differential equation:

$$\rho C_p \frac{\partial T}{\partial t} = \nabla.\left(k\nabla T\right) + \dot{Q} \quad \text{in } \Omega_{\text{BG}} \times [0, t_f]\,, \tag{1}$$

which is subjected to the initial and boundary conditions:

$$\begin{aligned} &T = T_0 \quad \text{at } t = 0, \quad \text{in } \Omega_{\text{BG}},\\ &T = \bar{T} \quad \text{on } \Gamma_T \times [0, t_f]\,,\\ &-k\nabla T.\hat{n} = \bar{q} \quad \text{on } \Gamma_q \times [0, t_f]\,, \end{aligned}$$

where ρ, C_p, and k are the density, specific heat capacity and conductivity of the solid, whereas T and $\dot{Q}$ are the temperature and heat source term, respectively. The temperature $\bar{T}$ and the heat flux $\bar{q}$ are prescribed at the non-overlapping boundaries Γ_T and Γ_q ($\Gamma_{\text{BG}} = \Gamma_T \cup \Gamma_q$), and $\hat{n}$ is the normal unit vector pointing outwards Γ_q. The solution of (1) is also subjected to the following CDC on the immersed boundary $\Gamma_{\text{PC}\to\text{BG}}$:

$$T = \bar{T}_{\text{PC}} \quad \text{on } \Gamma_{\text{PC}\to\text{BG}} \times [0, t_f] \ \text{(CDC)},$$

where $\bar{T}_{\text{PC}}$ is computed from the solution of a complementary transient heat conduction problem to be solved in the fine arrangement of patch nodes representing the domain Ω_{PC}, which moves with the heat source over Ω_{BG}. The complementary problem is described by the following partial differential equation, which includes an advective term in order to take into account the rigid motion of Ω_{PC} over the actual problem domain Ω_{BG}:

$$\rho C_p \frac{\partial T}{\partial t} - \rho C_p \vec{v}.\nabla T = \nabla.\left(k\nabla T\right) + \dot{Q} \quad \text{in } \Omega_{\text{PC}}, \tag{2}$$

where $\vec{v}$ is the velocity of Ω_{PC}. Eq. (2) can actually be conceived as an Arbitrary Lagrangian-Eulerian (ALE) description with a null material velocity [56], for the transient heat conduction problem to be solved over Ω_{PC}. This approach must not be confused with the Rosenthal's formulation, which is an approximation where the advective term arises because the transient heat conduction problem is described in a coordinates system attached to the moving heat source [7,57]. It should be emphasised that the heat source location is assumed to be fixed in the Rosenthal's approach, whereas the effects of its motion are introduced by the advective term. On the other hand, the heat source location is updated at each time step in the current Ov-IEFG approach. The advective term included in Eq. (2) is actually not related to a transformation of the transient heat conduction equation to a moving coordinates system whose location is subjected to the heat source motion, but to the ALE description inherent in the relative motion between the actual problem domain Ω_{BG} (whose material velocity is null) and the moving patch nodes representing Ω_{PC}. The solution of (2) is also subjected to the initial condition:

$$T = T_0 \quad \text{at } t = 0, \quad \text{in } \Omega_{\text{PC}},$$

and the following CDC on the immersed boundary $\Gamma_{\text{BG}\to\text{PC}}$:

$$T = \bar{T}_{\text{BG}} \quad \text{on } \Gamma_{\text{BG}\to\text{PC}} \times [0, t_f] \ \text{(CDC)}.$$

where $\bar{T}_{\text{BG}}$ is computed via the temperature approximations performed over the coarse background nodes arrangement, for the solution of Eq. (1). It is important to highlight the marked reciprocal dependence of Eqs.(1) and (2), given the need of imposing the CDC inherent in the transfer of information between the overlapping arrangements of nodes. The temperature $\bar{T}_{\text{PC}}$ to be imposed on the immersed boundary $\Gamma_{\text{PC}\to\text{BG}}$ for the solution of Eq.(1) is computed from the temperature approximations performed to solve Eq.(2), whereas the temperature $\bar{T}_{\text{BG}}$ to be imposed on the immersed boundary $\Gamma_{\text{BG}\to\text{PC}}$ for the solution of Eq.(2) is computed from the temperature approximations performed to solve Eq.(1). These features of the proposed Ov-IEFG approach lead to the need of performing an iterative procedure at each time step, until convergence is reached in the coupling between such complementary transient heat conduction equations for the definitive achievement of a single enriched solution. The iterative procedure will be conducted in the context of IEFG formulations developed for the solution of Eqs.(1) and (2) over the arrangements of background and patch nodes, respectively.

2.2. Formulation and iterative algorithm of the Ov-IEFG procedure

The Overset-IEFG procedure proposed in this communication is developed in terms of the weak formulations of Eqs.(1) and (2), which are given as follows:

$$\begin{aligned} &\int_{\Omega_{\text{BG}}} \delta T \rho\, C_p \frac{\partial T}{\partial t} \mathrm{d}\Omega + \int_{\Omega_{\text{BG}}} \nabla \delta T.k\nabla T \mathrm{d}\Omega\\ &= \int_{\Omega_{\text{BG}}} \delta T \dot{Q} \mathrm{d}\Omega + \int_{\Gamma_q} \delta T\, \bar{q}\, \mathrm{d}\Gamma + \int_{\Gamma_T} \delta T h_p \left(\bar{T} - T\right) \mathrm{d}\Gamma\\ &\qquad + \int\limits_{\Gamma_{\text{PC}\to\text{BG}}} \delta T h_p \left(\bar{T}_{\text{PC}} - T\right) \mathrm{d}\Gamma, \end{aligned} \tag{3}$$

$$\begin{aligned} &\int_{\Omega_{\text{PC}}} \delta T \rho\, C_p \frac{\partial T}{\partial t} \mathrm{d}\Omega + \int_{\Omega_{\text{PC}}} \nabla \delta T.k\nabla T \mathrm{d}\Omega\\ &- \int_{\Omega_{\text{PC}}} \delta T \rho\, C_p \vec{v}.\nabla T \mathrm{d}\Omega = \int_{\Omega_{\text{PC}}} \delta T \dot{Q} \mathrm{d}\Omega\\ &\qquad + \int\limits_{\Gamma_{\text{BG}\to\text{PC}}} \delta T h_p \left(\bar{T}_{\text{PC}} - T\right) \mathrm{d}\Gamma. \end{aligned} \tag{4}$$

In Eqs.(3) and (4), h_p is the penalty parameter concerning the imposition of Dirichlet conditions at both the external (Γ_T) and immersed coupling ($\Gamma_{\text{PC}\to\text{BG}}$ and $\Gamma_{\text{BG}\to\text{PC}}$) boundaries.

The IEFG formulation of (3) is obtained using the same IMLS approximations for both the temperature and its virtual variation, which are defined in terms of the coarse arrangement of background nodes concerning the fixed representation of the entire problem domain $\Omega_{\rm BG}$:

$$\delta T(\vec{x}) = \sum_{I=1}^{n_{\rm BG}} \varphi_{\rm BG}^{(I)}(\vec{x})\, \delta\hat{T}_{\rm BG}^{(I)}, \qquad T(\vec{x}) = \sum_{J=1}^{n_{\rm BG}} \varphi_{\rm BG}^{(J)}(\vec{x})\, \hat{T}_{\rm BG}^{(J)}, \quad (5)$$

where $n_{\rm BG}$ is the number of background nodes. On the other hand, the IEFG formulation of (4) involves IMLS approximations defined in terms of the fine arrangement of patch nodes representing the moving domain $\Omega_{\rm PC}$:

$$\delta T(\vec{x}) = \sum_{I=1}^{n_{\rm PC}} \varphi_{\rm PC}^{(I)}(\vec{x})\, \delta\hat{T}_{\rm PC}^{(I)}, \qquad T(\vec{x}) = \sum_{J=1}^{n_{\rm PC}} \varphi_{\rm PC}^{(J)}(\vec{x})\, \hat{T}_{\rm PC}^{(J)}, \quad (6)$$

where $n_{\rm PC}$ is the number of patch nodes.

The IMLS approximations to be used in this work are constructed over square influence domains with weight functions based on cubic splines, whereas the corresponding weighted orthogonal polynomial basis vectors are constructed from bilinear basis functions. A more comprehensive explanation about the construction of IMLS approximations with such features can be found in previous communications [42,43], whereby readers are referred to these work for further details in this regard. In order to simplify the notation, the argument $(\vec{x})$ of the IMLS approximations is omitted hereinafter.

The substitution of approximations (5) in (3) gives rise to the following IEFG formulation for the background nodes arrangement, which has been achieved preserving the fact that it must hold for any $\delta\hat{T}_{\rm BG}^{(I)}$:

$$\begin{aligned}
&\sum_{J=1}^{n_{\rm BG}} \underbrace{\left[\int_{\Omega_{\rm BG}} \varphi_{\rm BG}^{(I)} \rho\, C_p \varphi_{\rm BG}^{(J)}\, {\rm d}\Omega\right]}_{C_{IJ}^{\rm BG}} \dot{\hat{T}}_{\rm BG}^{(J)} \\
&+ \sum_{J=1}^{n_{\rm BG}} \underbrace{\left[\int_{\Omega_{\rm BG}} \nabla\varphi_{\rm BG}^{(I)}.k\nabla\varphi_{\rm BG}^{(J)}\, {\rm d}\Omega\right]}_{K_{IJ}^{\rm BG}} \hat{T}_{\rm BG}^{(J)} \\
&+ \sum_{J=1}^{n_{\rm BG}} \underbrace{\left[\int_{\Gamma_T} \varphi_{\rm BG}^{(I)} h_p \varphi_{\rm BG}^{(J)}\, {\rm d}\Gamma + \int_{\Gamma_{\rm PC\to BG}} \varphi_{\rm BG}^{(I)} h_p \varphi_{\rm BG}^{(J)}\, {\rm d}\Gamma\right]}_{P_{IJ}^{\rm BG}} \hat{T}_{\rm BG}^{(J)} \\
&= \underbrace{\left[\int_{\Omega_{\rm BG}} \varphi_{\rm BG}^{(I)} \dot{Q}\, {\rm d}\Omega\right]}_{F_I^{\rm BG(\dot{Q})}} + \underbrace{\left[\int_{\Gamma_q} \varphi_{\rm BG}^{(I)}\, \bar{q}\, {\rm d}\Gamma\right]}_{F_I^{\rm BG(\bar{q})}} \\
&\quad + \underbrace{\left[\int_{\Gamma_T} \varphi_{\rm BG}^{(I)} h_p \bar{T}\, {\rm d}\Gamma + \int_{\Gamma_{\rm PC\to BG}} \varphi_{\rm BG}^{(I)} h_p \bar{T}_{\rm PC}\, {\rm d}\Gamma\right]}_{F_I^{\rm BG(h_p)}}. \quad (7)
\end{aligned}$$

Similarly, the following IEFG formulation for the patch nodes arrangement is achieved after the substitution of approximations (6) in (4):

$$\begin{aligned}
&\sum_{J=1}^{n_{\rm PC}} \underbrace{\left[\int_{\Omega_{\rm PC}} \varphi_{\rm PC}^{(I)} \rho\, C_p \varphi_{\rm PC}^{(J)}\, {\rm d}\Omega\right]}_{C_{IJ}^{\rm PC}} \dot{\hat{T}}_{\rm PC}^{(J)} \\
&+ \sum_{J=1}^{n_{\rm PC}} \underbrace{\left[\int_{\Omega_{\rm PC}} \nabla\varphi_{\rm PC}^{(I)}.k\nabla\varphi_{\rm PC}^{(J)}\, {\rm d}\Omega\right]}_{K_{IJ}^{\rm PC}} \hat{T}_{\rm PC}^{(J)} \\
&- \sum_{J=1}^{n_{\rm PC}} \underbrace{\left[\int_{\Omega_{\rm PC}} \varphi_{\rm PC}^{(I)} \rho\, C_p \vec{v}.\nabla\varphi_{\rm PC}^{(J)}\, {\rm d}\Omega\right]}_{A_{IJ}^{\rm PC}} \hat{T}_{\rm PC}^{(J)} \\
&+ \sum_{J=1}^{n_{\rm PC}} \underbrace{\left[\int_{\Gamma_{\rm BG\to PC}} \varphi_{\rm PC}^{(I)} h_p \varphi_{\rm PC}^{(J)}\, {\rm d}\Gamma\right]}_{P_{IJ}^{\rm PC}} \hat{T}_{\rm PC}^{(J)} = \underbrace{\left[\int_{\Omega_{\rm PC}} \varphi_{\rm PC}^{(I)} \dot{Q}\, {\rm d}\Omega\right]}_{F_I^{\rm PC(\dot{Q})}} \\
&\qquad + \underbrace{\left[\int_{\Gamma_{\rm BG\to PC}} \varphi_{\rm PC}^{(I)} h_p \bar{T}_{\rm BG}\, {\rm d}\Gamma\right]}_{F_I^{\rm PC(h_p)}}. \quad (8)
\end{aligned}$$

The IEFG formulations given for each nodes distribution in (7) and (8) can be summarized as follows:

$$\begin{aligned}
&\sum_{J=1}^{n_{\rm BG}} C_{IJ}^{\rm BG} \dot{\hat{T}}_{\rm BG}^{(J)} + \sum_{J=1}^{n_{\rm BG}} \left(K_{IJ}^{\rm BG} + P_{IJ}^{\rm BG}\right) \hat{T}_{\rm BG}^{(J)} \\
&\qquad = F_I^{\rm BG(\dot{Q})} + F_I^{\rm BG(\bar{q})} + F_I^{\rm BG(h_p)}, \quad (9)
\end{aligned}$$

$$\begin{aligned}
&\sum_{J=1}^{n_{\rm PC}} C_{IJ}^{\rm PC} \dot{\hat{T}}_{\rm PC}^{(J)} + \sum_{J=1}^{n_{\rm PC}} \left(K_{IJ}^{\rm PC} - A_{IJ}^{\rm PC} + P_{IJ}^{\rm PC}\right) \hat{T}_{\rm PC}^{(J)} \\
&\qquad = F_I^{\rm PC(\dot{Q})} + F_I^{\rm PC(h_p)}, \quad (10)
\end{aligned}$$

and finally re-written in the following arrangements of matrices and vectors:

$$\begin{aligned}
&\mathbf{C}^{\rm BG}\dot{\hat{\mathbf{T}}}^{\rm BG} + \left(\mathbf{K}^{\rm BG} + \mathbf{P}^{\rm BG}\right) \hat{\mathbf{T}}^{\rm BG} \\
&\qquad = \mathbf{F}^{\rm BG(\dot{Q})} + \mathbf{F}^{\rm BG(\bar{q})} + \mathbf{F}^{\rm BG(h_p)}, \quad (11)
\end{aligned}$$

$$\begin{aligned}
&\mathbf{C}^{\rm PC}\dot{\hat{\mathbf{T}}}^{\rm PC} + \left(\mathbf{K}^{\rm PC} - \mathbf{A}^{\rm PC} + \mathbf{P}^{\rm PC}\right) \hat{\mathbf{T}}^{\rm PC} \\
&\qquad = \mathbf{F}^{\rm PC(\dot{Q})} + \mathbf{F}^{\rm PC(h_p)}. \quad (12)
\end{aligned}$$

The transient problem involved in Eqs. (11) and (12) will be solved at each time step under a fully implicit backward finite difference scheme, which gives rise to the following algebraic systems of equations:

$$\begin{aligned}
&\left(\frac{\mathbf{C}^{\rm BG}}{\Delta t} + \mathbf{K}^{\rm BG} + \mathbf{P}^{\rm BG}\right) \hat{\mathbf{T}}^{\rm BG}\Big|_{t+\Delta t} = \frac{\mathbf{C}^{\rm BG}}{\Delta t}\, \hat{\mathbf{T}}^{\rm BG}\Big|_{t} \\
&\qquad + \left(\mathbf{F}^{\rm BG(\dot{Q})} + \mathbf{F}^{\rm BG(\bar{q})} + \mathbf{F}^{\rm BG(h_p)}\right)\Big|_{t+\Delta t}, \quad (13)
\end{aligned}$$

$$\left(\frac{\mathbf{C}^{\mathrm{PC}}}{\Delta t}+\mathbf{K}^{\mathrm{PC}}-\mathbf{A}^{\mathrm{PC}}+\mathbf{P}^{\mathrm{PC}}\right)\hat{\mathbf{T}}^{\mathrm{PC}}\Big|_{t+\Delta t} = \frac{\mathbf{C}^{\mathrm{PC}}}{\Delta t}\hat{\mathbf{T}}^{\mathrm{PC}}\Big|_{t}+\left(\mathbf{F}^{\mathrm{PC}(\dot{Q})}+\mathbf{F}^{\mathrm{PC}(h_p)}\right)\Big|_{t+\Delta t}. \quad (14)$$

The reciprocal dependence of Eqs. (1) and (2) has now been settled in terms of the iterative solution of the algebraic systems of equations (13) and (14), which are coupled via the load vectors $\mathbf{F}^{\mathrm{PC}(h_p)}$ and $\mathbf{F}^{\mathrm{BG}(h_p)}$. The nodal parameters of vector $\hat{\mathbf{T}}_{\mathrm{PC}}$ are used to compute the temperature $\bar{T}_{\mathrm{PC}}$ involved in the assembling of $\mathbf{F}^{\mathrm{BG}(h_p)}$, whereas the vector $\hat{\mathbf{T}}_{\mathrm{BG}}$ is used to calculate the temperature $\bar{T}_{\mathrm{BG}}$ required for the assembling of $\mathbf{F}^{\mathrm{PC}(h_p)}$. According to the features described so far, the Ov-IEFG procedure proposed in this communication is implemented according to the algorithm schematized in the following flowchart in pseudo code:

1. Inizialization of $\hat{\mathbf{T}}_{\mathrm{BG}}\Big|_t$ and $\hat{\mathbf{T}}_{\mathrm{PC}}\Big|_t$ according to the initial condition $T=T_0$. Assembling of (13) and (14).
2. Iterative Ov-IEFG procedure: set $\omega=0$, $\hat{\mathbf{T}}^{(\omega)}_{\mathrm{BG}}\Big|_{t+\Delta t} = \hat{\mathbf{T}}_{\mathrm{BG}}\Big|_t$ and $\hat{\mathbf{T}}^{(\omega)}_{\mathrm{PC}}\Big|_{t+\Delta t} = \hat{\mathbf{T}}_{\mathrm{PC}}\Big|_t$.
   (a)
   - if $\omega \geq 1$, $\bar{T}^{(\omega+1)}_{\mathrm{PC}} = \bar{T}^{(\omega)}_{\mathrm{PC}}$.
   - Otherwise, no CDC should be imposed on $\Gamma_{\mathrm{PC-BG}}$

   (b) Solving (13): $\hat{\mathbf{T}}_{\mathrm{BG}}\Big|_t$, $\hat{\mathbf{T}}^{(\omega)}_{\mathrm{BG}}\Big|_{t+\Delta t} \rightarrow \hat{\mathbf{T}}^{(\omega+1)}_{\mathrm{BG}}\Big|_{t+\Delta t}$.
   (c) Computing $\bar{T}^{(\omega+1)}_{\mathrm{BG}}$ using (5) on $\Gamma_{\mathrm{BG-PC}}$.
   (d) Solving (14): $\hat{\mathbf{T}}_{\mathrm{PC}}\Big|_t$, $\hat{\mathbf{T}}^{(\omega)}_{\mathrm{PC}}\Big|_{t+\Delta t} \rightarrow \hat{\mathbf{T}}^{(\omega+1)}_{\mathrm{PC}}\Big|_{t+\Delta t}$.
   (e) Computing $\bar{T}^{(\omega+1)}_{\mathrm{PC}}$ using (6) on $\Gamma_{\mathrm{PC-BG}}$.
   (f) Stop criterion:
   - if $\omega=0$, $\omega \leftarrow \omega+1$, go back to (a).
   - Otherwise:
     - if $\|\bar{T}^{(\omega+1)}_{\mathrm{BG}} - \bar{T}^{(\omega)}_{\mathrm{BG}}\|_{\mathrm{L}^2(\Gamma_{\mathrm{BG-PC}})} + \|\bar{T}^{(\omega+1)}_{\mathrm{PC}} - \bar{T}^{(\omega)}_{\mathrm{PC}}\|_{\mathrm{L}^2(\Gamma_{\mathrm{PC-BG}})} \geq \epsilon$, $\omega \leftarrow \omega+1$, then go back to (a).
     - Otherwise, set $t \leftarrow t+\Delta t$, $\hat{\mathbf{T}}_{\mathrm{BG}}\Big|_t = \hat{\mathbf{T}}^{(\omega+1)}_{\mathrm{BG}}\Big|_{t+\Delta t}$, and $\hat{\mathbf{T}}_{\mathrm{PC}}\Big|_t = \hat{\mathbf{T}}^{(\omega+1)}_{\mathrm{PC}}\Big|_{t+\Delta t}$, and go to the next time step (g).

   (g) Next time step:
   - if $t < t_f$, Assemble (13) and (14), and then go back to (2).
   - Otherwise, got to (3).
3. Compute the temperature distributions T_{BG} in $\Omega_{\mathrm{BG}}-\Omega_{\mathrm{PC}}$ using (5), and T_{PC} in Ω_{PC} using (6). Obtain the effective solution of the heat transfer problem as $T = T_{\mathrm{BG}} \cup T_{\mathrm{PC}}$.

3. Model description and numerical results

The Ov-IEFG procedure will be tested in a problem with the configuration depicted in Fig.2, which is a useful benchmark case to prove the suitability of alternative numerical techniques to conduct an appropriate analysis of the transient heat conduction phenomena with moving heat sources involved in arc welding processes [7,33]. The figure represents a thin plate subjected to an arc welding process, where the heat source moves with constant velocity $\vec{v}=(u,0)$ along the horizontal axis of symmetry.

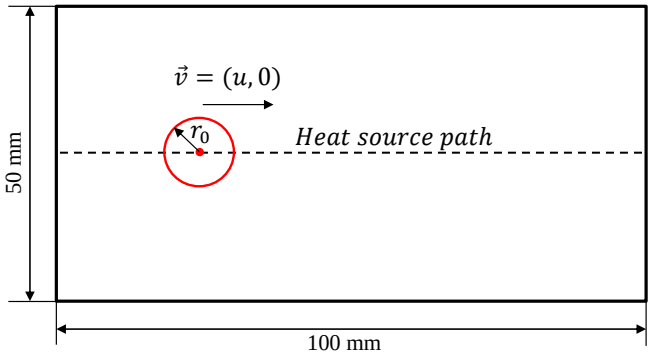

Figure 2: Physical and geometric features of the heat transfer problem concerning a thin plate subjected to an arc welding process with the heat source following a straight path along the horizontal axis of symmetry.

The heat source is considered to have an effective circular area where the power density is distributed according to [7,33]:

$$\dot{Q} = \dot{Q}_0 e^{-r^2/r_0^2}. \quad (15)$$

In (15) $\dot{Q}_0$ is the maximum power density at the heat source centre times the plate thickness, r is the distance from the heat source centre, and r_0 is a radius defining an effective circular area such that:

$$Q_T = \dot{Q}_0 \pi r_0^2 = 2\pi \int_0^\infty \dot{Q}_0 e^{-r^2/r_0^2}\, r\mathrm{d}r, \quad (16)$$

Eq. (16) is written considering that r_0 defines an effective circular area where a uniform heat source of value $\dot{Q}_0$ would provide the whole power Q_T of the Gaussian distribution given by (15). According to the symmetries inherent in the problem configuration, the numerical solutions will be conducted over the upper half of the plate subjected to the boundary conditions depicted in Fig.3.

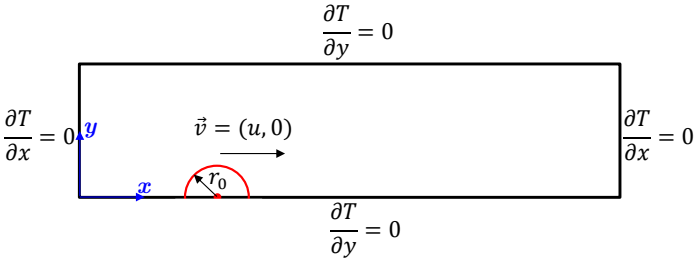

Figure 3: Computational domain and boundary conditions to be imposed in the numerical solution of the heat transfer problem with the configuration depicted in Fig.2.

The current problem only involves adiabatic boundary conditions on Γ_{BG}, i.e. $\bar{q} = 0$ on Γ_q and $\Gamma_T = \emptyset$. The transient heat conduction problem will be solved considering the welding parameters and material properties summarized in Table 1, with the initial position of the heat source centre at $(x_s, y_s) = (0, 0)$.

Table 1: Welding parameters and material properties for the transient heat conduction problem of the thin plate subjected to an arc welding process with the heat source following a straight path along the horizontal axis of symmetry.

Welding parameters	Values
Plate length (mm)	100
Plate width (mm)	50
Total power of the Gaussian source Q_T (W)	62.83185
Initial temperature T_0 (°C)	0
Heat source speed u (mm/s)	2
Material properties	**Values**
Conductivity (W.mm^{-1}.K^{-1})	0.025
Specific heat capacity (J.kg^{-1}.K^{-1})	658
Density (kg.mm^{-3})	7.6×10^{-6}

In order to demonstrate the positive features about using the proposed Ov-IEFG procedure in the analysis of transient heat conduction with moving heat sources, the current case will be solved for heat sources of increasingly smaller effective radii. The total power of the Gaussian source is kept constant, whereby the maximum power density of the source for each case is computed as:

$$\dot{Q}_0 = \frac{Q_T}{\pi r_0^2}.$$

The total power for the Gaussian source given in Table 1 has been determined taking as reference an effective circular area of radius $r_0 = 2$ mm with a maximum power density times the plate thickness of $\dot{Q}_0 = 5$ W.mm^{-2}, which corresponds to the arc welding parameters considered in the numerical studies conducted by Pham [7] and Reséndiz Flores-Saucedo Zendejo [33]. The proposed Ov-IEFG technique has been used to solve such a transient heat conduction problem with moving heat source, considering effective circular areas with radius of 2 mm, 0.2 mm and 0 mm (point heat source). The arrangements of overlapping nodes corresponding to different instants of the transient heat conduction analysis are depicted in Fig.4(a)-(c), where the patch nodes moves according to the heat source path.

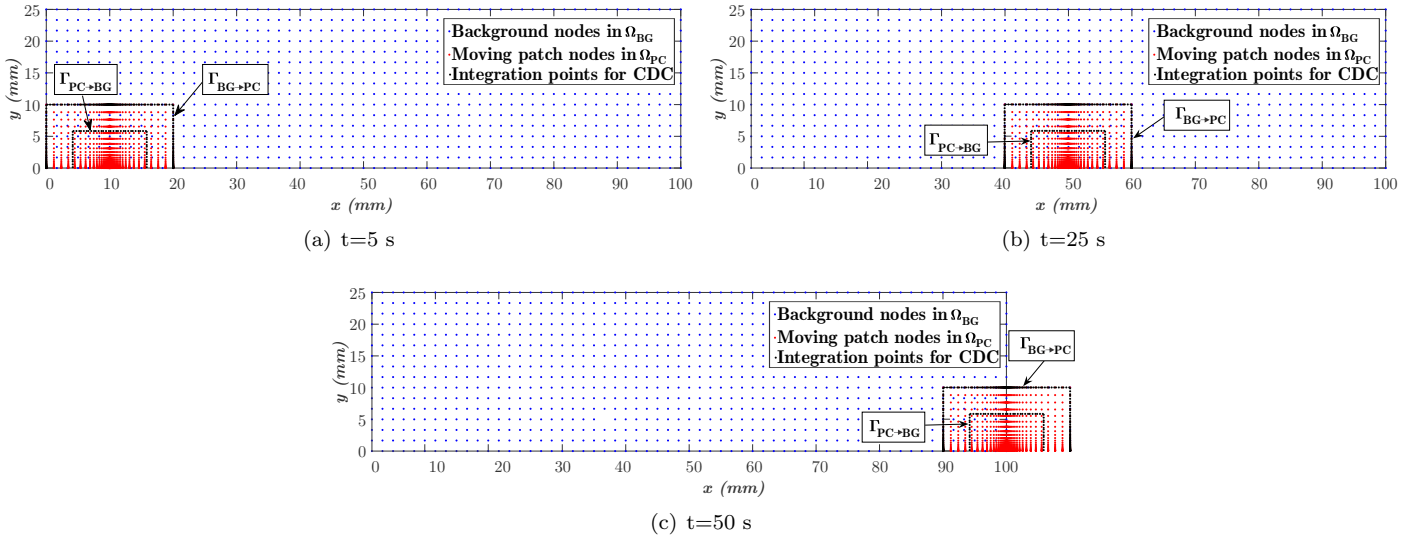

(a) t=5 s

(b) t=25 s

(c) t=50 s

Figure 4: Overlapping nodes arrangement used in the solution of the heat transfer problem over the rectangular thin plate. The patch nodes (red) move with the heat source, and the integrals corresponding to the transfer of information via the CDC are computed using the Gauss integration points (black) lying on the embedded boundaries $\Gamma_{\text{BG}\to\text{PC}}$ and $\Gamma_{\text{PC}\to\text{BG}}$.

The temperature distributions computed via the Ov-IEFG approach for each size of effective circular area are depicted in Fig.5(a)-(c), Fig.6(a)-(c) and Fig.7(a)-(c), whereas a comparison between the corresponding temperature profiles computed along the horizontal axis of symmetry is given in Fig.8(a)-(c). Although the solutions have been performed in the computational domain depicted in Fig.3, the corresponding temperature distributions have been plotted over the entire plate for a better visualization. The smooth and stable temperature distributions achieved under the proposed Ov-IEFG technique demonstrate the potential of this numerical approach to properly capture the marked thermal gradients developed near the moving heat source, regardless the size of its effective area. The temperature profiles along the horizontal axis of symmetry exhibit a continuous and smooth transition in the region of coupling between

both nodes arrangements, which proves that transferring information through the immersed boundaries $\Gamma_{BG\to PC}$ and $\Gamma_{PC\to BG}$ using the penalty method involved in the Ov-IEFG formulation is actually an accurate and reliable procedure of straightforward implementation. The distribution of moving patch nodes used in this problem has been fine enough to allow an appropriate capture of the moving heat source effects not only in the case of an effective area of moderate dimensions ($r_0 = 2$ mm), but also for the more demanding situations of small effective area ($r_0 = 0.2$ mm) and point heat source ($r_0 = 0$ mm).

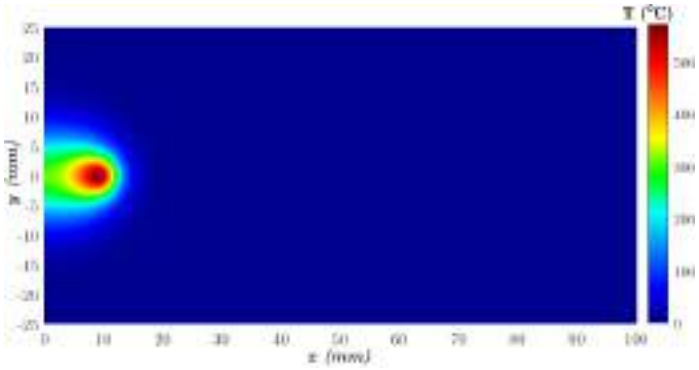

(a) t=5 s

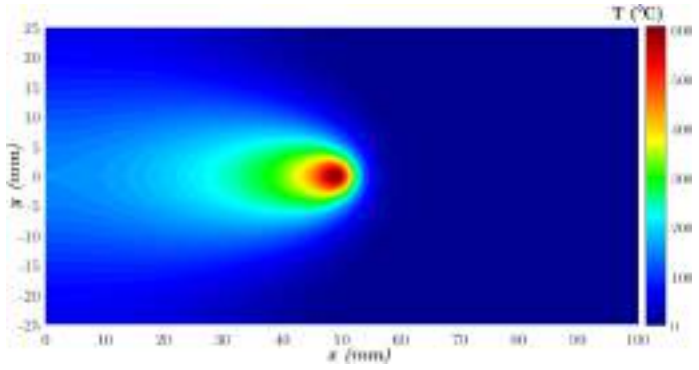

(b) t=25 s

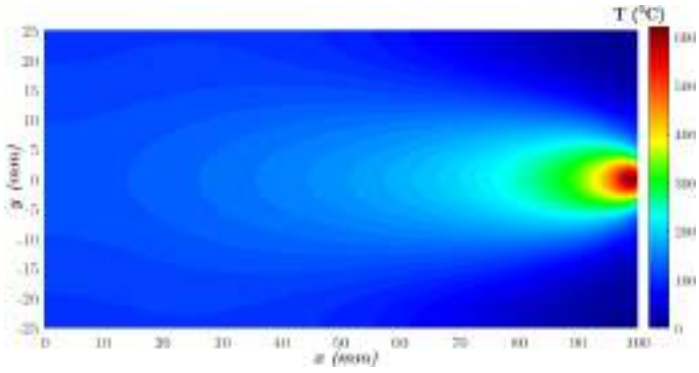

(c) t=50 s

Figure 5: Temperature distributions computed over the rectangular plate at different times via the proposed Ov-IEFG, with a moving heat source of an effective circular area of radius $r_0 = 2$ mm.

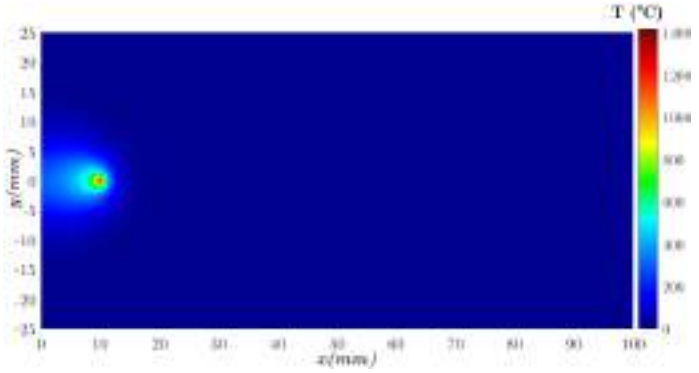

(a) t=5 s

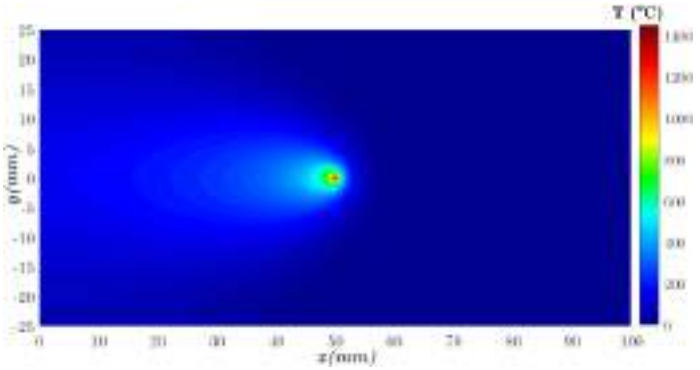

(b) t=25 s

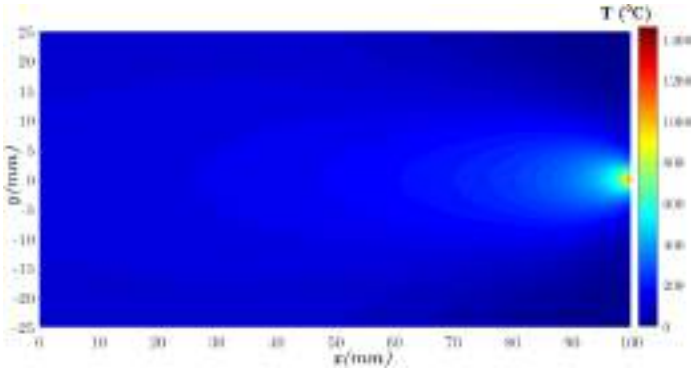

(c) t=50 s

Figure 6: Temperature distributions computed over the rectangular plate at different times via the proposed Ov-IEFG, with a moving heat source of an effective circular area of radius $r_0 = 0.2$ mm.

The moving and background computational domains have been represented with 51×26 and 61×16 nodes, respectively. Additionally, the moving patch nodes have been clustered near the heat source centre via the coordinates transformation used by Ding [58]. The results exhibit a noteworthy increment in temperature and the corresponding gradients in the moving heat source vicinity as the effective radius for energy distribution gets smaller until the extreme situation of point heat source is reached, for which the maximum temperature computed via the Ov-IEFG approach exceeds 6000 °C.

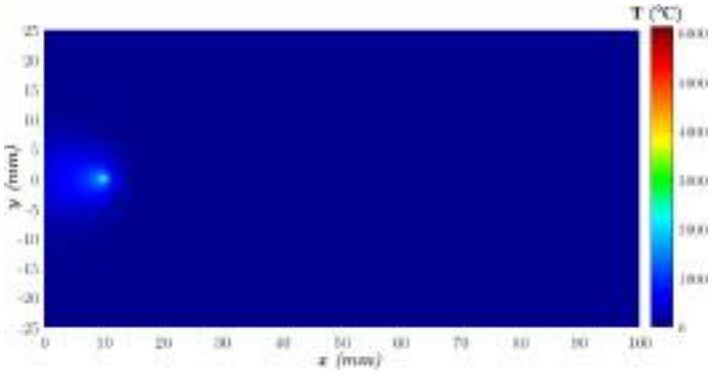

(a) t=5 s

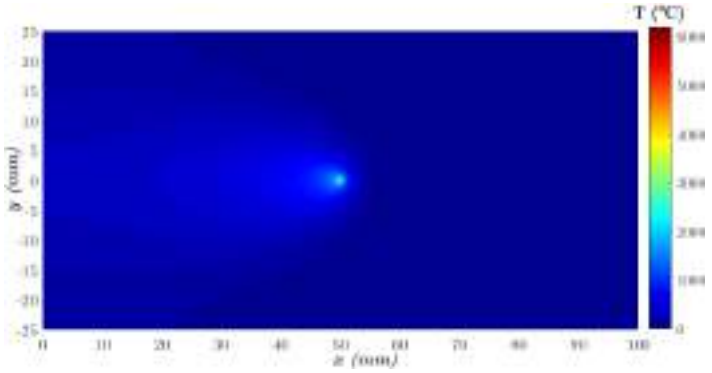

(b) t=25 s

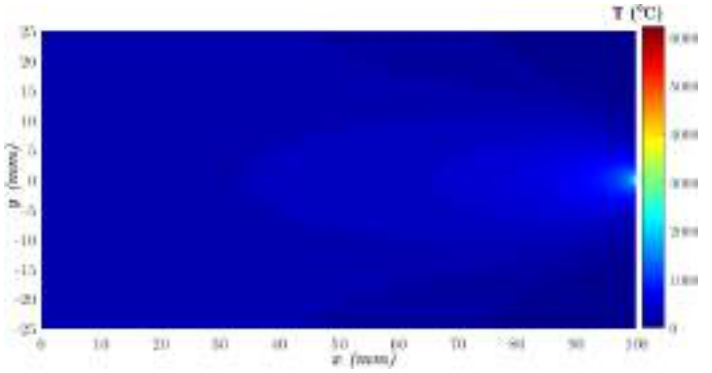

(c) t=50 s

Figure 7: Temperature distributions computed over the rectangular plate at different times via the proposed Ov-IEFG, with a moving heat source of an effective circular area of radius $r_0 = 0$ mm (point heat source).

Although the approximation enrichment performed via the moving patch nodes has allowed the prediction of a remarkably high temperature at the point heat source location at each time step, it is worth mentioning that achieving convergence to a finite value of temperature at such a position is actually unfeasible. This is because the temperature distribution under such extreme situation must formally reach an infinite value at the point heat source location at each time, which is demonstrated in the analytical solutions available in the pioneer work developed by Jaeger [59] and Rosenthal [57]. Moving point heat sources do not occur in reality, but are commonly used to approximately model heat sources of very small effective area [34,53,54].

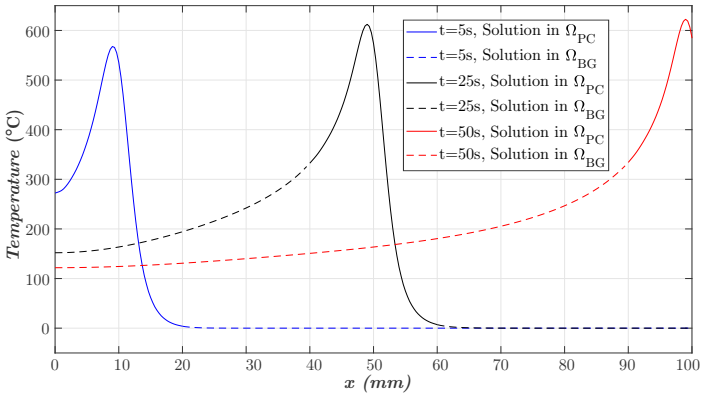

(a) $r_0 = 2$ mm

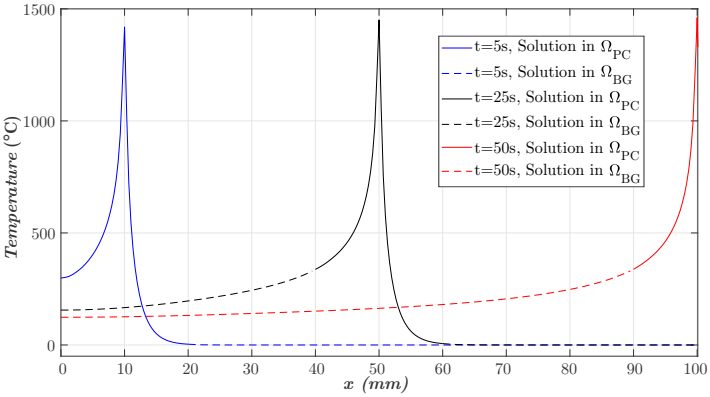

(b) $r_0 = 0.2$ mm

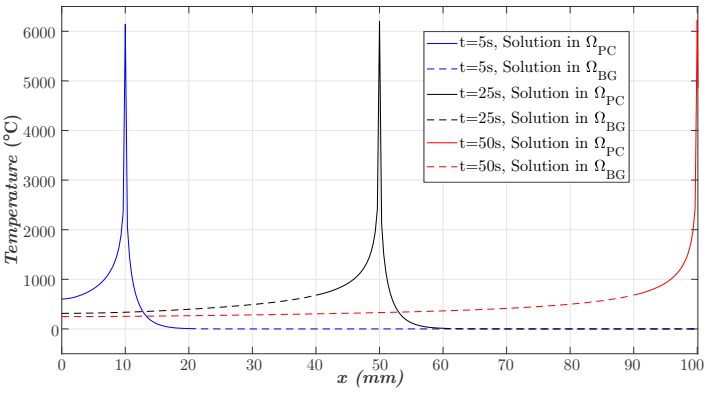

(c) $r_0 = 0$ mm (point heat source)

Figure 8: Temperature profiles computed at different times along the horizontal symmetry axis of the plate, via the proposed Ov-IEFG.

Although the temperature computed at the exact location of the moving point heat source does not actually provide any meaningful information, the appropriate capture of the markedly high thermal gradients developed near it demands strict requirements of accuracy and stability of the numerical technique used to perform an appropriate analysis of the transient heat conduction process. The

numerical results obtained via the Ov-IEFG technique in the moving point heat source case demonstrate the robustness and stability of such an approach, since -even under such extreme conditions- it has also given rise to an stable and detailed capture of the temperature distributions and marked thermal gradients developed in the heat source vicinity followed by an smooth and continuous transition in the region of coupling between both arrangements of nodes.

The results reported so far demonstrate that the Ov-IEFG approach allows an accurate computation of the marked temperature increments and corresponding gradients developed in the moving heat sources vicinity without resorting to an adaptive nodes refinement, but only a fine enough arrangement of patch nodes moving with the heat source. Such patch nodes arrangement reciprocally transfer information with the coarse distribution of background nodes in order to achieve the enriched final solutions reported so far, in a remarkably simple manner.

4. Discussion

The results reported in the previous section have put in an appropriate perspective the suitability of using the current Ov-IEFG to obtain accurate solutions for transient heat conduction problems with a moving heat source inherent in arc welding processes, in a remarkably simple manner. The IMLS approximations using nodes in a moving local support domain allows a straightforward and high-order continuous computation of the temperature throughout the entire problem domain, whereas the fine distribution of moving patch nodes leads to an enriched approximation of temperature in the heat source vicinity in order to achieve an accurate integration of the thermal energy delivered to the plate. The integrals given in the IEFG formulations (7) and (8) have been computed via 3 Gauss quadrature rules (9 points in each integration cell) individually defined for the background and moving patch nodes, and the integration cells are defined in terms of the nodes position. The Gauss points in Ω_{BG} are fixed, whereas the Gauss points in Ω_{PC} undergo the same rigid body motion of the patch nodes. Such feature allows a fairly simple computation of the integrals inherent in the Ov-IEFG procedure at each time step, when compared to the procedures required to conform the density of integration points to the nodes position in the framework of meshless solutions with adaptive nodes refinement [34]. It should be mentioned that the smooth transition of the temperature distributions in the region of coupling between both arrangements of nodes has also been achieved via an appropriate selection of the immersed boundary locations, which must be defined such that the distance between $\Gamma_{\mathrm{BG}\rightarrow\mathrm{PC}}$ and $\Gamma_{\mathrm{BG}\rightarrow\mathrm{PC}}$ is 2 to 3 times the nodal spacing of the background nodes arrangement representing Ω_{BG}. This has actually been conceived as an extension of the criterion introduced by Storti et al. [55] for overset techniques developed within the framework of FEM, which establishes that the achievement of a smooth coupling based on the local implementation of high-order interpolation schemes requires a distance between immersed boundaries of at least twice the average size of the background mesh elements in the coupling region. Particularly in this work, the support size of the nodal influence domains used to construct the IMLS has been chosen to be twice the spacing between neighbouring nodes, whereas the distance between $\Gamma_{\mathrm{BG}\rightarrow\mathrm{PC}}$ and $\Gamma_{\mathrm{BG}\rightarrow\mathrm{PC}}$ is 2.5 times the nodal spacing. Such support size gives rise to a fairly smooth and continuous high-order approximation of temperature, which has allowed the appropriate extension of the Storti et al. [55] criterion to the meshless Ov-IEFG approach proposed in this communication. The fine distribution of moving patch nodes used in the current Ov-IEFG approach has allowed the achievement of the accurate results reported so far, in a remarkably simple manner. The significance of such a positive feature is depicted in Fig.9(a)-(c), where the temperature profiles computed at $t = 25$ s via the Ov-IEFG procedure along the thin plate horizontal axis of symmetry are compared to standard IEFG-based solutions performed using uniform distributions of nodes to represent the problem domain. The Ov-IEFG technique performs significantly better than the IEFG method formulated under a single uniform distribution of fixed nodes, since the last has exhibited noteworthy difficulties concerning the appropriate capture of the moving heat source effects. The Ov-IEFG technique has given rise to an appropriate capture of the high temperatures and marked thermal gradients developed in the moving heat source vicinity, whereas the standard IEFG formulation has not allowed such straightforward achievement of accurate results in the more demanding situations of small effective area and point heat source. The temperature profiles achieved via the Ov-IEFG technique in the case of an effective area of moderate dimensions ($r_0 = 2$ mm) are virtually indistinguishable from those computed via the standard IEFG method based on a single uniform distribution of fixed nodes, regardless such fixed arrangements of nodes are coarse (61×16) or fine (201×51). This is a feature already discussed in the introduction of this communication, i.e. the smooth-higher order approximations achieved via IMLS are enough to achieve accurate results in the framework of meshless techniques when the heat source effective area has moderate dimensions [7,8,10,33]. On the other hand, such positive features concerning the IMLS approximations have not been enough to provide the same accuracy in the cases of small effective areas and point heat sources. In the particular case of the moving heat source with an small effective are of radius $r_0 = 0.2$ mm, the standard IEFG solution has required a domain representation consisting of $201 \times 51 = 10251$ nodes in order to roughly reach the accuracy achieved with the Ov-IEFG procedure proposed in this work. Such an outcome demonstrates the potential and suitability of the current approach to efficiently achieve accurate and stable approximations of temperature and heat flux in the heat source vicinity, since the number of nodes required in the standard IEFG solution exceeds 4 times the quantity used under the Ov-IEFG approach ($61\times16+51\times26 = 2302$).

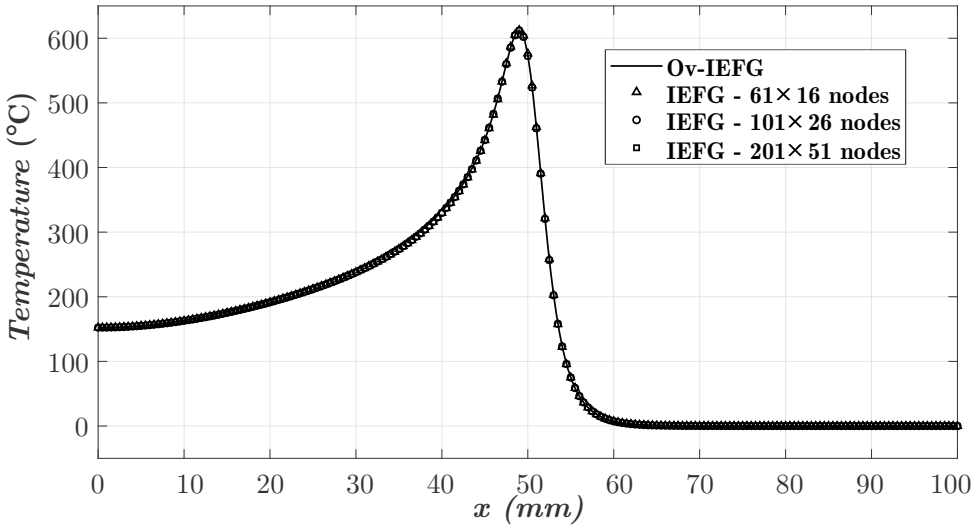

(a) $r_0 = 2$ mm

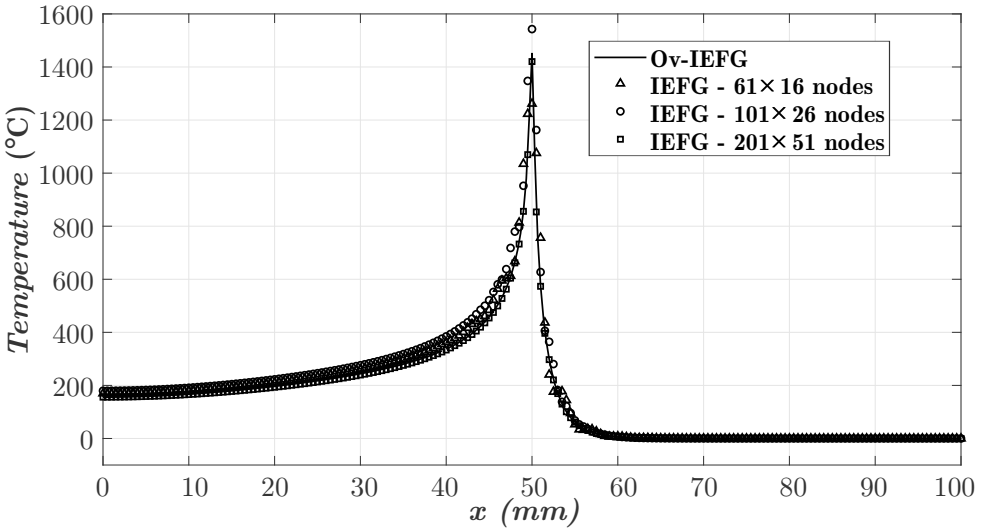

(b) $r_0 = 0.2$ mm

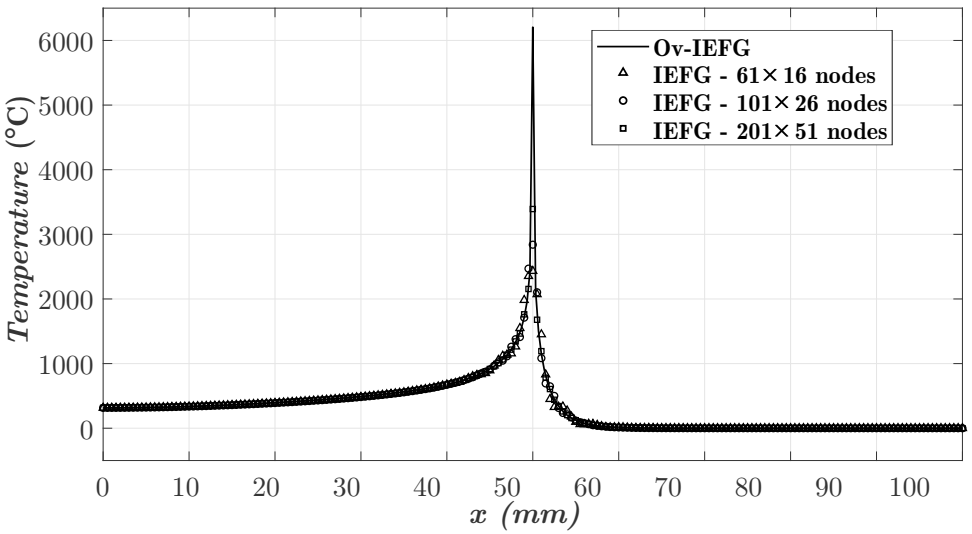

(c) $r_0 = 0$ mm (point heat source)

Figure 9: Comparison between the temperature profiles computed via the Ov-IEFG technique along the horizontal symmetry axis of the plate at $t = 25$ s, with those achieved via a standard IEFG method under increasingly refined uniform nodes distributions.

Furthermore, the standard IEFG-based formulation with a fine distribution of 201×51 fixed nodes in the moving point heat source situation still provides a very poor capture of the high temperatures and marked thermal gradients that must arise near such an extremely concentrated heat source, in comparison with the enriched solution performed via the proposed Ov-IEFG technique.

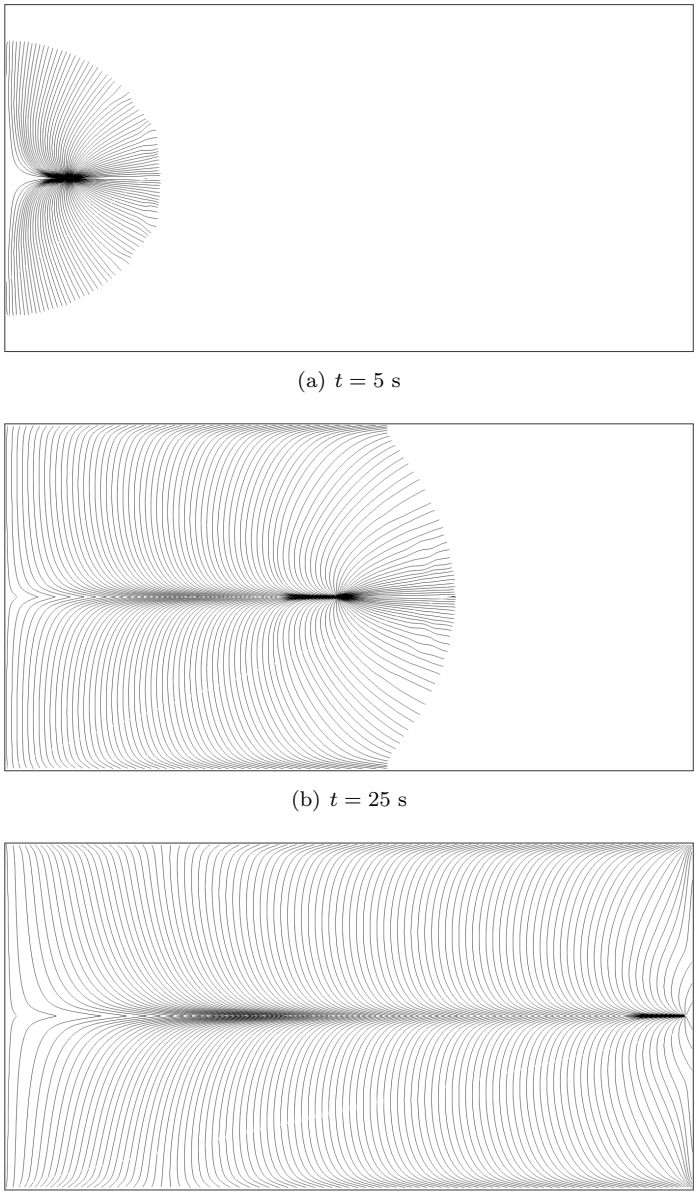

(a) $t = 5$ s

(b) $t = 25$ s

(c) $t = 50$ s

Figure 10: Heatlines patterns obtained over the rectangular plate at different times via the proposed Ov-IEFG, with a moving heat source of an effective circular area of radius $r_0 = 2$ mm.

These outcomes demonstrate the noteworthy potential of the Ov-IEFG technique to provide a more comprehensive use of the IMLS approximations positive features in the solution of transient heat conduction problems with moving heat sources, unlike the work so far available in the literature concerning fixed-nodes meshless procedures limited to the solution of problems involving moving heat sources with effective areas of moderate dimensions [7,8,10,33]. The current Ov-IEFG has also allowed a straightforward achievement of a smooth and continuous temperature distribution in the transition from Ω_{BG} to Ω_{PC}, which has already been depicted in Fig.5-8. This is possible due the continuous imposition of the CDC via the penalty integrals included in (7) and (8), which are computed capturing and continuously weighting information of neighbouring nodes defining a moving local support domain to construct the IMLS approximations at the integrations points along the immersed boundaries $\Gamma_{\mathrm{BG}\to\mathrm{PC}}$ and $\Gamma_{\mathrm{PC}\to\mathrm{BG}}$.

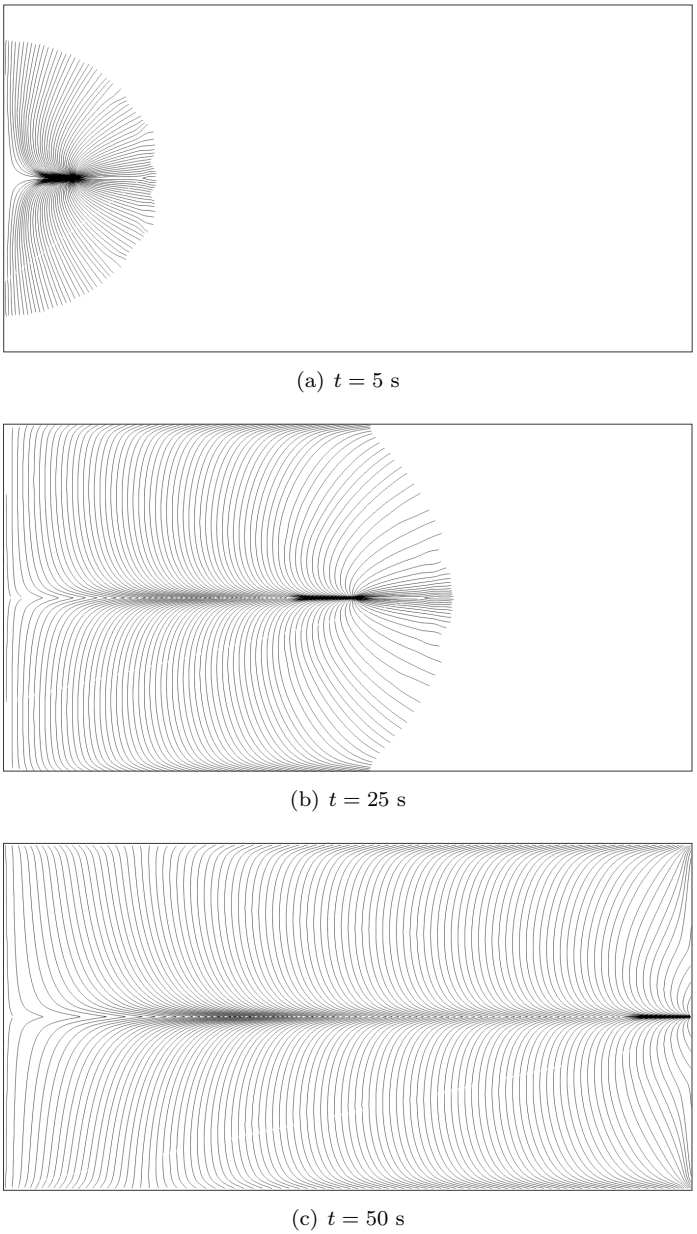

(a) $t = 5$ s

(b) $t = 25$ s

(c) $t = 50$ s

Figure 11: Heatlines patterns obtained over the rectangular plate at different times via the proposed Ov-IEFG, with a moving heat source of an effective circular area of radius $r_0 = 0.2$ mm.

(a) $t = 5$ s

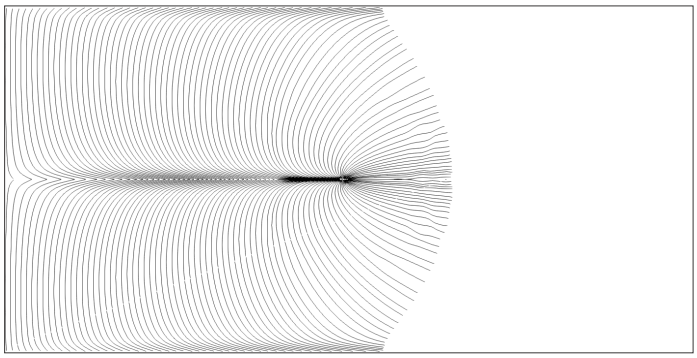

(b) $t = 25$ s

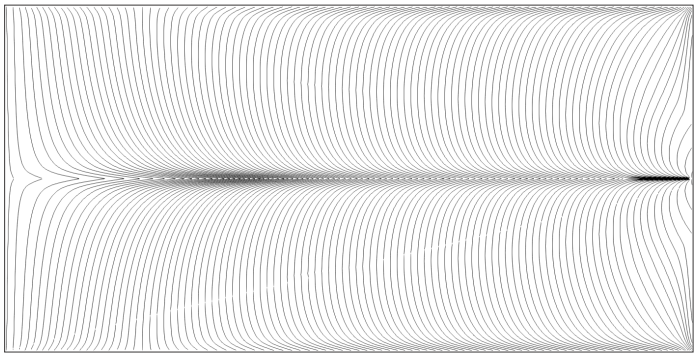

(c) $t = 50$ s

Figure 12: Heatlines patterns obtained over the rectangular plate at different times via the proposed Ov-IEFG, with a moving heat source of an effective circular area of radius $r_0 = 0$ mm. (point heat source)

Such a feature gives rise to a robust coupling of temperature and heat flux between both arrangements of nodes, since the information to be transferred along the immersed boundaries is directly computed at each integration point from a continuous and smooth field constructed via IMLS approximations. This is a fundamental difference with respect to nodes-based piecewise transfer of information commonly performed with the overset techniques developed for mesh-based methods, which usually involves a further local reconstruction procedure conceived to enrich the information to be transferred between overlapping meshes or grids in order to allow a smooth coupling [55].

The positive features of the IMLS approximations have not only allowed the achievement of smooth and stable distributions of temperature, but also of conductive heat flux. This outcome is demonstrated in the heatlines depicted in Fig.10(a)-(c), Fig.11(a)-(c) and Fig.12(a)-(c), which have been constructed for each size of effective circular area.

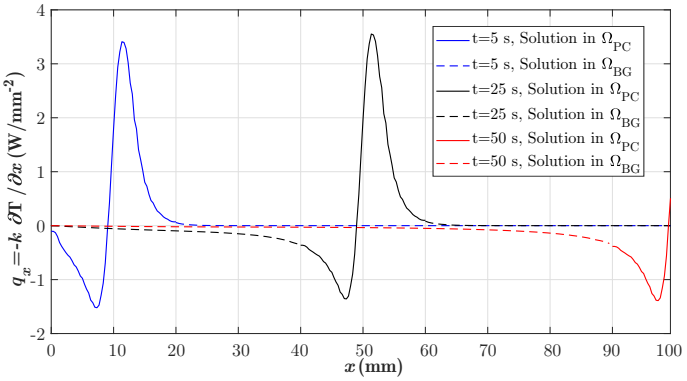

(a) $r_0 = 2$ mm

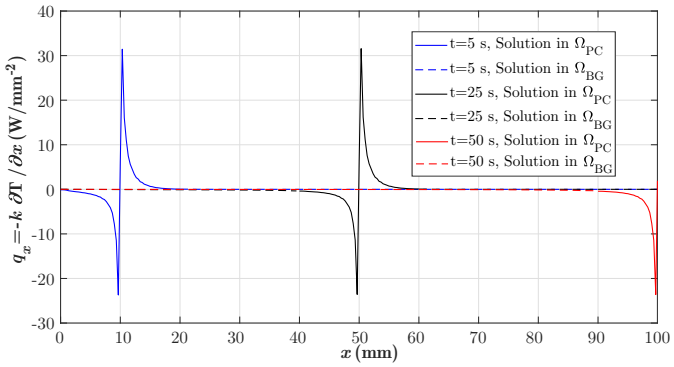

(b) $r_0 = 0.2$ mm

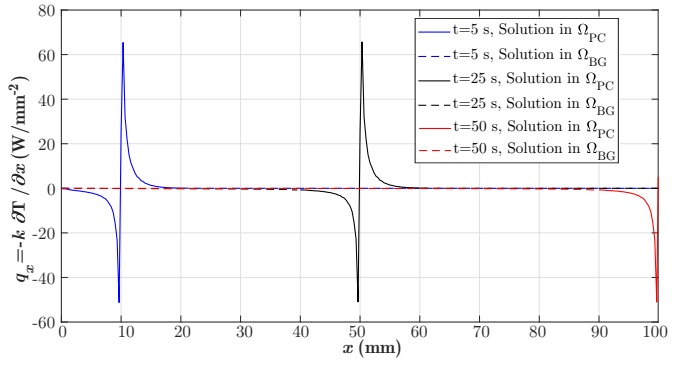

(c) $r_0 = 0$ mm (point heat source)

Figure 13: Profiles of the horizontal heat flux component computed at different times along the horizontal symmetry axis of the plate, via the proposed Ov-IEFG.

The heatlines are smooth and stable in most of the plate, and exhibit some slight fluctuations in regions upstream the moving heat source at $t = 5$ s and $t = 25$ s. The heat flux is extremely low in such regions, which have not yet perceived the moving heat source pass. Constructing heat-

lines in regions where the heat flux is virtually uniform and null do not provide meaningful physical insights concerning the heat transfer problem, and such information will be unaccurate regardless the numerical technique used. This aspect provides an explanation to the slight fluctuations of some heatlines upstream the moving heat source, and why the heatlines have not been plotted over the entire plate at $t = 5$ s and $t = 25$ s. The smooth and stable heatlines computed via the Ov-IEFG technique are actually related to the potential of this numerical approach to properly capturing the high temperature gradients near the moving heat source, which gives rise to a stable and accurate computation of the heat flux via the Fourier's Law. The heatlines do not exhibit spurious oscillations or discontinuities in the transition from Ω_{BG} to Ω_{PC}, which is not an easy task in the framework of overset methods. This outcome demonstrates the possibility of performing an accurate and straightforward transfer not only of thermal information via the proposed Ov-IEFG technique, but also of the corresponding thermal gradients. A better visualization of the smooth heat flux transition in the coupling between Ω_{BG} and Ω_{PC} is given in Fig.13(a)-(c), where the horizontal component of the computed heat fluxes ($q_x = -k\,\partial T/\partial x$) have been plotted along the horizontal symmetry axis of the plate. Regardless the radius of the heat source effective area, the Ov-IEFG technique has given rise to a smooth coupling between the heat flux profiles computed in Ω_{BG} (dashed lines) and Ω_{PC} (solid lines). The conductive heat fluxes in Ω_{BG} and Ω_{PC} have been computed and coupled in a straightforward manner, by introducing the IMLS given in (5) and (6) in the Fourier's Law:

$$\vec{q} = -k\nabla T = \begin{cases} -k\displaystyle\sum_{I=1}^{n_{\mathrm{BG}}} \nabla\varphi_{\mathrm{BG}}^{(I)}(\vec{x})\hat{T}_{\mathrm{BG}}^{(I)} & \text{in } \Omega_{\mathrm{BG}} \\ \\ -k\displaystyle\sum_{I=1}^{n_{\mathrm{PC}}} \nabla\varphi_{\mathrm{PC}}^{(I)}(\vec{x})\hat{T}_{\mathrm{PC}}^{(I)} & \text{in } \Omega_{\mathrm{PC}} \end{cases} . \qquad (17)$$

Accordingly, the smooth and continuous derivatives inherent in the IMLS approximations have allowed the direct coupling of the heat fluxes computed in Ω_{BG} and Ω_{PC} via (17). Such a feature demonstrates that the proposed Ov-IEFG approach has a noteworthy potential to provide a straightforward construction of both enriched temperature and heat flux distributions, via a straightforward IMLS-based coupling between the solutions computed in Ω_{BG} and Ω_{PC}. This is actually different from the overset techniques developed in the context of mesh-based methods, where the discontinuous element-wise or cell-wise approximations of the spatial derivatives precludes to perform a continuous coupling between the heat fluxes computed in the patch and background meshes or grids. Such issue is usually solved setting the final global enriched solution over a single mesh or grid reconstructed from the patch and background meshes or grids, which is performed via the substitution of overlapping regions with non-structured grids. The reconstructed mesh or grid keeps the nodal values of the non substituted elements or cells, and the enriched heat flux field is computed performing the temperature derivatives over such single mesh [55].

4.1. Suitability of the Ov-IEFG procedure in cases of heat sources moving along curve paths

The proposed Ov-IEFG technique have been used so far in the solution of transient heat conduction problems concerning arc welding processes with moving heat sources following a straight path, which is enough to put in an appropriate perspective the potential and reliability of this approach to achieve stable and accurate results for both temperature and heat flux in the vicinity of moving heat sources of any size (even point heat sources). It is worth to mention that in cases of heat sources following such a simple path, the heat transfer problem can also be accurately solved performing an appropriate refinement of the domain discretization along the heat source path. Such kind of refinements are not feasible in the framework of problems with moving heat sources following curve or arbitrary paths, whereby complex and robust remeshing or nodes reconfiguration algorithms are required in these situations. The current section is focused on using the proposed Ov-IEFG technique to solve a transient heat conduction problem with a point heat source moving along a curve path, in a remarkably simple manner. The solution of such a problem is intended to put in an appropriate perspective an additional positive feature of the Ov-IEFG method, which is the possibility of achieving accurate and stable numerical results without the need of resorting to remeshing or nodes reconfiguration procedures conceived to properly capture the effects of heat sources moving along curve paths. This positive feature will be demonstrated solving a heat conduction problem with the geometry and boundary conditions depicted in Fig.14, and the results will be compared to the solution performed by Khosravifard et al. [34] via a RPIM with adaptive nodes reconfiguration. In this problem, the heat source position $\vec{x}_s(t)$ at time t is given by:

$$\vec{x}_s(t) = \begin{cases} x_s(t) = \frac{3t}{5000} + 1 \text{ (m)}, \\ \\ y_s(t) = \frac{1}{9}\left[\left(\frac{3t}{5000}+1\right)^2 - 2\left(\frac{3t}{5000}+1\right) + 10\right] \text{ (m)}, \end{cases} \quad 0 \le t \le 5000 \text{ (s)} \qquad (18)$$

whereby the heat source moves with a velocity $\vec{v}(t) = (u_s(t), v_s(t))$ given by:

$$\vec{v}(t) = \begin{cases} u_s(t) = \frac{3}{5000} \text{ (m/s)}, \\ \\ v_s(t) = \frac{2t}{5000^2} \text{ (m/s)}, \end{cases} \quad 0 \le t \le 5000 \text{ (s)} \qquad (19)$$

The current problem involves both Dirichlet and Neumann boundary conditions on Γ_{BG}, which are $\bar{q} = 0$ on Γ_q and $\bar{T} = 200$ K on Γ_T. The transient heat conduction problem will be solved considering the welding parameters and material properties summarized in Table 2, with the initial position of the heat source centre at $(x_s, y_s) = (1, 1)$ (m).

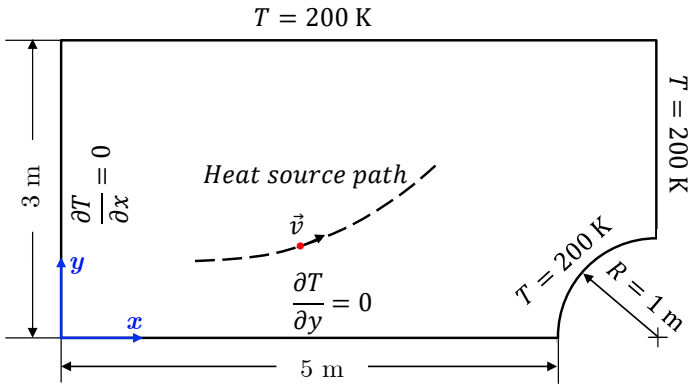

Figure 14: Geometry and boundary conditions concerning the heat conduction problem with a moving heat source following a curve path, in this case the heat source velocity is not constant.

Table 2: Welding parameters and material properties concerning the transient heat conduction problem with a moving heat source following a curve path, proposed by Khosravifard et al. [34].

Welding parameters	Values
Total power of the point heat source Q_T (W)	20000
Initial temperature T_0 (K)	200
Material properties	**Values**
Conductivity (W.m^{-1}.K^{-1})	54
Specific heat capacity (J.kg^{-1}.K^{-1})	465
Density (kg.m^{-3})	7833

The arrangements of overlapping nodes at times t = 2500 s and t = 5000 s are depicted in Fig.15(a)-(b), where the patch nodes moves following the curve path of the moving heat source. The moving and background computational domains have been represented with 1270 and 1681 nodes, respectively. The corresponding temperature distributions are given in Fig.16(a)-(b), and the results achieved near the heat source via the proposed Ov-IEFG approach exhibit a markedly smoother and more stable behaviour than those reported by Khosravifard et al. [34]. It is also worth mentioning that the maximum temperature computed under Ov-IEFG approach actually exceeds the upper limit of the colours scale, but it has been set in order to perform a fair qualitative comparison with the temperature distributions of Khosravifard et al. [34]. Such a feature is put in a better perspective in Fig.17, which includes the temperature profiles computed along the horizontal lines y = 1.9 m, y = 1.99 m and y = 2.0 m at t=5000 s. The maximum value of temperature in the profile corresponding to the line passing over the current position of the heat source $(x_s, y_s) = (4, 2)$ (m) is 388 K, and the results exhibit a continuous and smooth coupling between Ω_{BG} (dashed lines) and Ω_{PC} (solid lines). It is also worth to mention in this case that the temperature computed at the exact location of the moving point heat source does not actually provide any meaningful information, but it is also noteworthy that the Ov-IEFG approach has allowed a stable and detailed capture of the temperature increments and marked thermal gradients developed in the heat source vicinity. Such outcomes demonstrate the noteworthy potential of the Ov-IEFG technique to achieve accurate and stable results in the solution of transient heat conduction problems inherent in arc welding processes, regardless the moving heat source path.

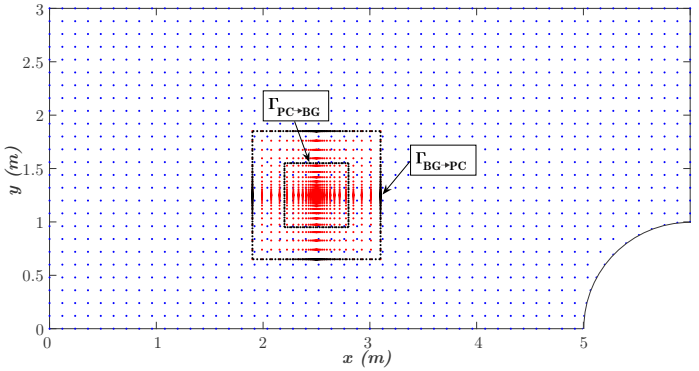

(a) t=2500 s

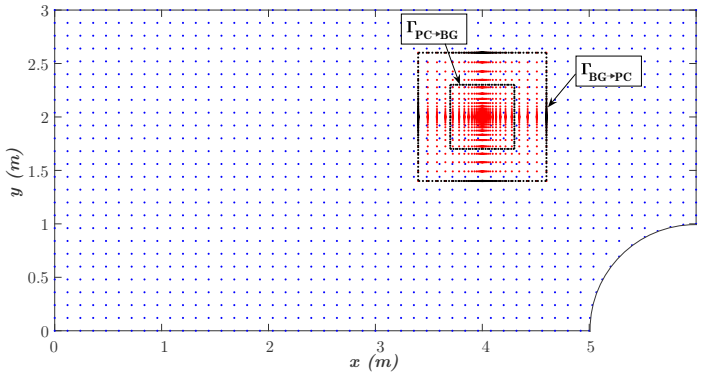

(b) t=5000 s

Figure 15: Overlapping nodes arrangement used in the solution of the heat transfer problem with moving heat source following a curve path. The patch nodes (red) move with the heat source, and the integrals corresponding to the transfer of information via the CDC are computed using the Gauss integration points (black) lying on the embedded boundaries $\Gamma_{\mathrm{BG}\to\mathrm{PC}}$ and $\Gamma_{\mathrm{PC}\to\mathrm{BG}}$.

The smoothness and stability of the temperature distributions achieved via the proposed Ov-IEFG approach are related to an appropriate selection of the influence domain for each node according to the local average nodal spacing of the non-uniform distribution used to represent Ω_{PC}, where the nodes are exponentially clustered near to the heat source via the coordinates transformation given in the work of Ding. [58]. A comprehensive explanation concerning a simple procedure to define the influence domain of each node in these kind of clustered distributions can be found in a previous communication [43]. The appropriate selection of the influence domains has been performed only once and kept during the entire analysis of the transient heat conduction problem, since the patch nodes arrangement undergoes a simple rigid body motion following the heat source.

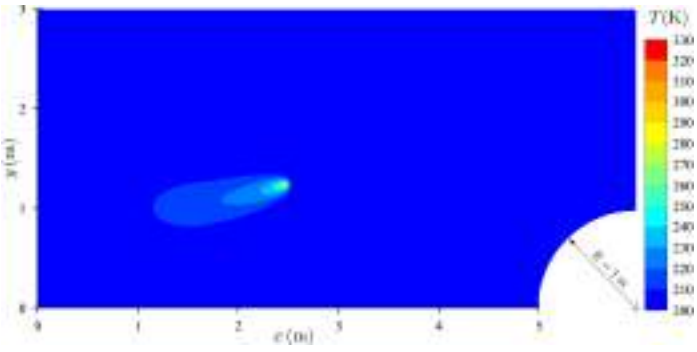

(a) t=2500 s

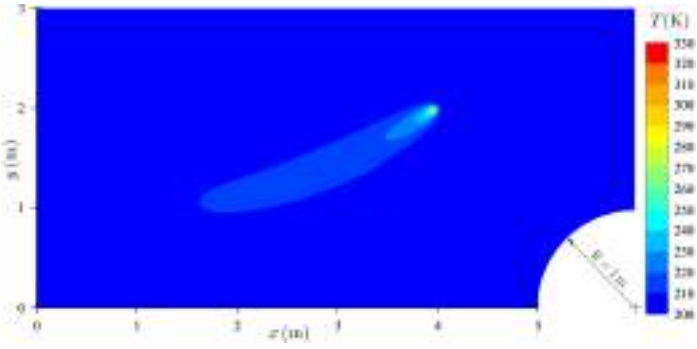

(b) t=5000 s

Figure 16: Temperature distributions concerning the Ov-IEFG-based solution of the heat transfer problem with moving point heat source following a curve path, at times 2500 s and 5000 s.

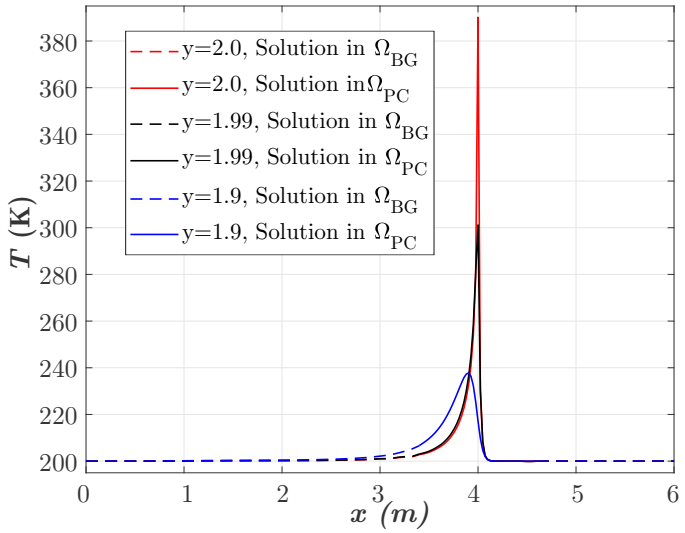

Figure 17: Temperature profile along the horizontal line $y = 1.9$ m, $y = 1.99$ m and $y = 2.0$ m at t=5000 s.

This feature is a crucial implementation advantage over the dynamic nodes reconfiguration procedure used in the RPIM-BDM-based solution performed in [34], where both defining the nodal influence domains and conforming the integration points to the nodes distribution at each time step are cumbersome and computing demanding procedures. The temperature profile computed along the horizontal line $y = 1.9$ m at t=5000 s using the proposed Ov-IEFG method is compared in Fig.18 with the results achieved by Khosravifard et al. [34] via the dynamic nodes reconfiguration procedure and the RPIM-BDM, and the solutions exhibit an excellent fitting. Such results demonstrate the accuracy and reliability of the solutions achieved via the Ov-IEFG procedure proposed in this work, now in the context of transient heat conduction problems with heat sources moving along curve paths.

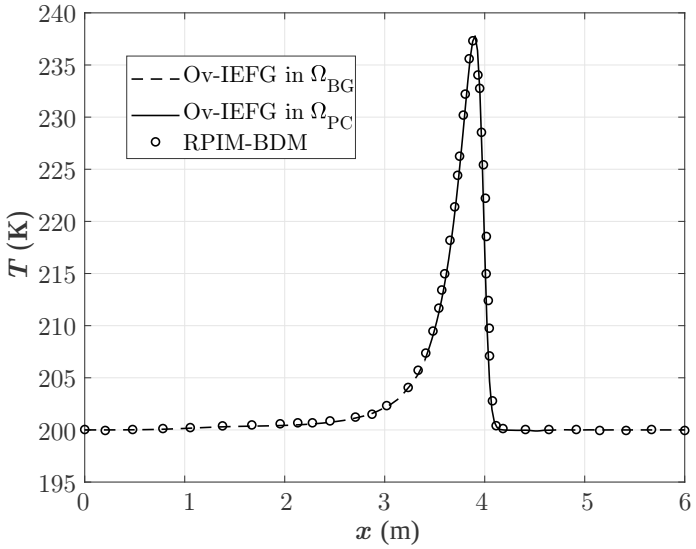

Figure 18: Comparison of the temperature profile computed via the Ov-IEFG technique along the horizontal line $y = 1.9$ m at t=5000 s, with the RIPM-based solution subjected to the adaptive nodes refinement proposed by Khosravifard et al. [34].

4.2. Accuracy and computing performance

The aspects discussed so far regarding the Ov-IEFG method performance have put into proper perspective the potential of this novel approach in the solution of transient conduction heat transfer problems with moving heat sources following both straight and curved paths, where the arrangements of moving patch nodes have allowed an appropriate capture of the high temperatures and marked thermal gradients developed in the vicinity of heat sources with effective areas of any size. The possibility of improving the accuracy of an IEFG-based solution to capture the moving heat source effects via the Ov-IEFG approach proposed in this work has been demonstrated within the framework of a simple benchmark involving a rectangular thin plate with a heat source moving with constant velocity along the horizontal axis of symmetry, where the Ov-IEFG technique has allowed an appropriate capture of the high temperature and marked thermal gradients developed near the moving heat source. Actually, it was demonstrated that the proposed approach is remarkably more accurate than a standard IEFG method formulated under a single uniform

nodes distribution. The Ov-IEFG approach has been subsequently implemented in the solution of a more complex problem involving a point heat source moving with variable velocity along a curve path in a not rectangular geometry, and the results achieved have exhibited an excellent agreement with the solution performed by Khosravifard et al. [34] under a RPIM with adaptive nodes reconfiguration. The rigid body motion of the patch nodes arrangement according to the heat source path allows the achievement of accurate results without resorting to procedures of nodal influence domains updating and integration points conforming, which are commonly required within the framework of adaptive nodes reconfiguration approaches [14,34].

Although the suitability and reliability of the proposed Ov-IEFG have already been demonstrated in the solution of problems where the moving heat source location in the problem domain is actually followed and updated at each time step, such a technique can also be implemented within the framework of a simple Rosenthal's formulation. This approach is a feasible approximation in regular geometry problems with moving heat sources following sufficiently simple paths so that no information about the current location of the heat source is required to perform an appropriate prediction of the temperature distribution developed around it, which allows a simple description of the transient heat conduction problem in a coordinates system attached to the moving heat source. This aspect allows the assumption of a fixed location for the moving heat source, whereas its motion is emulated via an advective term arising from the Rosenthal's coordinates transformation [7,57]. The numerical solution of transient heat conduction problems with moving heat sources under such approximated approach is remarkably simple, and its controlled conditions and low computing requirements make it suitable to conduct comprehensive parametric analyses in order to validate the accuracy of a proposed method. Particularly in the case of meshless methods, examples of accuracy analyses performed under the Rosenthal's formulation can be found in the work of Pham et al. [7] and Reséndiz Flores-Saucedo Zendejo [33]. Accordingly, a comprehensive parametric analysis within the framework of a Rosenthal's formulation will be conducted in the current section in order to validate the accuracy and assess the computing performance of the proposed Ov-IEFG technique. The aforementioned parametric analysis will be performed revisiting the simple benchmark case of the rectangular thin plate with a moving heat source following a horizontal straight path at constant velocity, now formulated under the Rosenthal's coordinates transformation. A fixed location at $(x, y) = (50, 0)$ (mm) for the moving heat source is assumed, and the fine arrangement of patch nodes is placed at such position in order to properly capture the temperature increments and marked thermal gradients developed near the moving heat source. An Ov-IEFG technique devised to solve transient heat conduction problems with moving heat sources under the Rosenthal's formulation is actually very simple to implement since both Ω_{BG} and Ω_{PC} are now fixed in space, and the thermal problems over each one of these overlapping domains are described in a coordinate system attached to the moving heat source. The partial differential equation to be solved in both Ω_{BG} and Ω_{PC} are the same as Eq. (2), but the advective term is now included in order to emulate appropriately the heat source motion according to the Rosenthal's coordinates transformation and not following an ALE description (there is no relative motion between Ω_{PC} and Ω_{BG}). The accuracy analysis is carried out by comparison with a FEM-based solution, which has been performed with a highly refined mesh such that the results achieved are accurate enough to be considered as benchmark. The mesh used for such FEM-based benchmark solution consists of $400 \times 100 = 4 \times 10^4$ elements exponentially clustered towards the heat source location, as depicted in Fig.19.

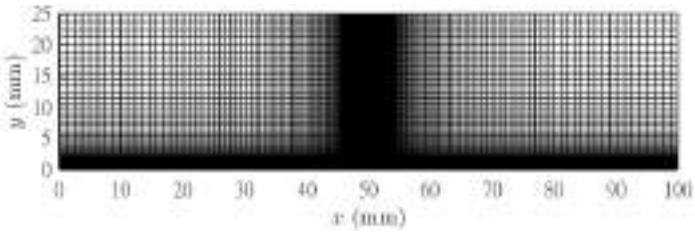

Figure 19: Fine mesh concerning the FEM-based benchmark solution.

The welding parameters and materials properties are the same given in Tab.1, and the effective circular area of the moving heat source has a radius of $r_0 = 0.002$ mm. The high accuracy of the FEM-based solution with the discretisation of Fig.19 is ensured since the increase in internal energy per unit thickness of the plate at every time instant is virtually non-sensitive to further mesh refinements, which is depicted in the asymptotic behaviour exhibited in Fig.20(a)-(c). Accordingly, the FEM-based solution of the current transient heat conduction problem with such mesh provides a very accurate capture of the energy delivered by the moving heat source. The accuracy of both the proposed Ov-IEFG approach and a standard IEFG method formulated under a single nodes distribution has been assessed in terms of the following normalized errors based on the L_2-norm, which have been computed with respect to the highly refined FEM-based benchmark solution:

$$E_{\mathrm{L}_2}^{\text{Ov-IEFG}} = \frac{\left\| T^{\text{Ov-IEFG}} - T^{\text{FEM}} \right\|_{\mathrm{L}_2}}{\left\| T^{\text{FEM}} \right\|_{\mathrm{L}_2}}, \tag{20}$$

$$E_{\mathrm{L}_2}^{\text{IEFG}} = \frac{\left\| T^{\text{IEFG}} - T^{\text{FEM}} \right\|_{\mathrm{L}_2}}{\left\| T^{\text{FEM}} \right\|_{\mathrm{L}_2}}. \tag{21}$$

The Ov-IEFG-based solutions have been performed under the same approach followed so far, i.e. a coarse uniform background nodes arrangement with a non-uniform fine patch nodes distribution overlapped at the moving heat source location and clustered towards its centre.

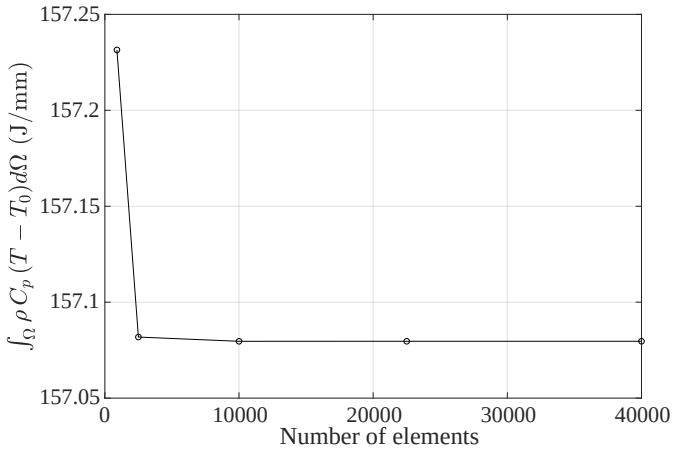

(a) t=5 s

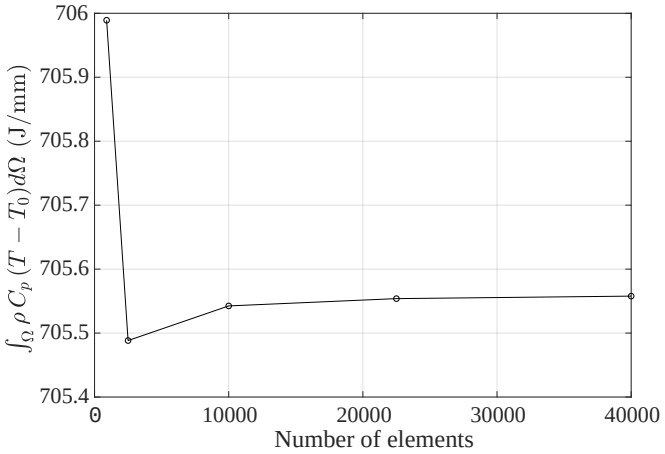

(b) t=25 s

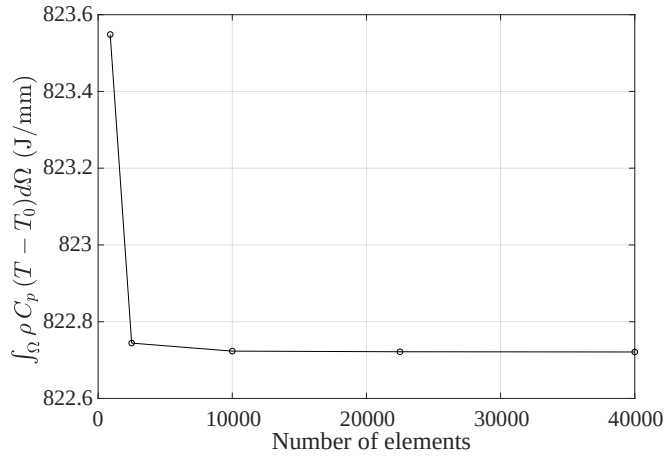

(c) t=50 s

Figure 20: Increase in internal energy per unit thickness of the plate computed via the FEM-based solution, for different mesh refinements at (a) t=5 s, (b) t=25 s, and (c) t=50 s. T_0 is the intial temperature of the plate

On the other hand, the distributions of nodes concerning the standard IEFG-based solutions have been subjected to the same exponential clustering performed towards the moving heat source location in the highly refined FEM-based benchmark solution. For visualization purposes, the finest nodes distributions used in the accuracy analysis of both the Ov-IEFG and standard IEFG approaches are shown in Fig.21(a)-(b).

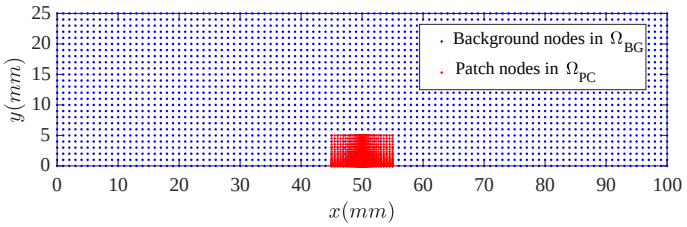

(a) Ov-IEFG

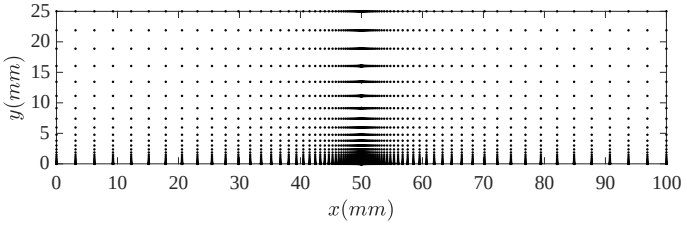

(b) IEFG

Figure 21: Finest nodes distributions used in the accuracy analysis of both the Ov-IEFG and standard IEFG approaches. The arrangements of nodes depicted for (a) the Ov-IEFG and (b) the standard IEFG approches consist of $101 \times 26 + 101 \times 51 = 7777$ and $161 \times 41 = 6601$ nodes, respectively.

The results achieved for different times are shown in Fig.22(a)-(c), which exhibit similar behaviour in the convergence of both methods to the highly refined FEM-based benchmark results. The numerical solutions have been performed under a fully implicit backward finite difference scheme with a time step of $\Delta t = 6.25 \times 10^{-4}$, and the behaviour of both the Ov-IEFG and standard IEFG-based solutions are similar in the course of the entire transient heat conduction analysis. Such an outcome demonstrates the significant potential of the proposed Ov-IEFG approach, since it allows the use of a very simple arrangement of background nodes with a very fine distribution of patch nodes particularly overlapped at the region of interest (the moving heat source location) to achieve an accuracy similar to that of a standard IEFG-based solution where the nodes distribution has been clustered appropriately near the heat source. It is also worth noting that the convergence behaviour of the Ov-IEFG slightly degrades with respect to the standard IEFG for the finest nodes distributions, and the standard IEFG with the clustered nodes distribution proves to be more accurate for domain representations consisting of more than about 5000 nodes. The plots of Fig.22(a)-(c) also exhibit similar convergence rates in terms of the number of nodes for both the Ov-IEFG and standard IEFG approaches. Both methods also exhibit convergence rates higher than those corresponding to a standard mesh-based

solution performed via FEM, which is a thoroughly studied positive feature of EFG methods [14]. For reference, the theoretical convergence rate in terms of the number of nodes for a FEM-based solution has been included in the convergence plots. Nevertheless, the convergence rate achieved according to the nodes refinement performed within the framework of the proposed Ov-IEFG technique is not as regular as that exhibited by the standard IEFG approach. The aforementioned aspects concerning the convergence behaviour of the Ov-IEFG technique are related to the penalty-based coupling between the arrangements of background and patch nodes involved in the proposed Ov-IEFG approach, which precludes the achievement of conventional convergence behaviours theoretically dictated in the context of standard meshless methods based on a single nodes distribution [14]. Such effects introduced by the CDC involved in the Ov-IEFG approach are subjected to several factors such as the support size of the nodal influence domains, the ratio between sizes of Ω_{PC} and Ω_{BG}, and the penalty factor used in the imposition of the CDC. Particularly in this work, the size of Ω_{PC} has been chosen to be 10 times the spacing between nodes of the coarse background arrangement used to represent Ω_{BG}, the support size of the nodal influence domains is twice the spacing between neighbouring nodes, and the penalty factor has been computed as $h_p = 100 \times k\, h^{-2}$ (h is the average spacing between neighbouring nodes of the background arrangement representing Ω_{BG}) [60]. The smoothness and accuracy of the results achieved so far in the solution of problems involving moving heat sources of different sizes following both straight and curve paths demonstrate that the aforementioned parameters have been appropriately setted, also leading to the achievement of a convergence behaviour similar to that of a standard IEFG-based solution performed under a single nodes distribution clustered near the moving heat source. A more comprehensive parametric analysis concerning the factors involved in the CDC can be conducted in order to get a more regular convergence behaviour, which is an interesting issue to be addressed in further work.

Although the standard IEFG formulation under the clustered nodes distribution exhibits a slightly better performance than the proposed Ov-IEFG approach for domain representations consisting of more than about 5000 nodes, to perform an appropriate nodes clustering is an easy task only in the current benchmark case where a fixed position for the moving heat source can be assumed according to the Rosenthal's coordinates transformation. On the other hand, the standard IEFG formulation could not be suitable within the framework of problems where the approximated approach of Rosenthal is not feasible and the moving heat source location must actually be followed. The implementation of dynamic nodes reconfiguration algorithms would be required to cluster properly the nodes distribution near the heat source at each time step, which -as discussed so far- is also subjected to the need of updating the nodal influence domains and conforming the integration points according to the nodes reconfiguration.

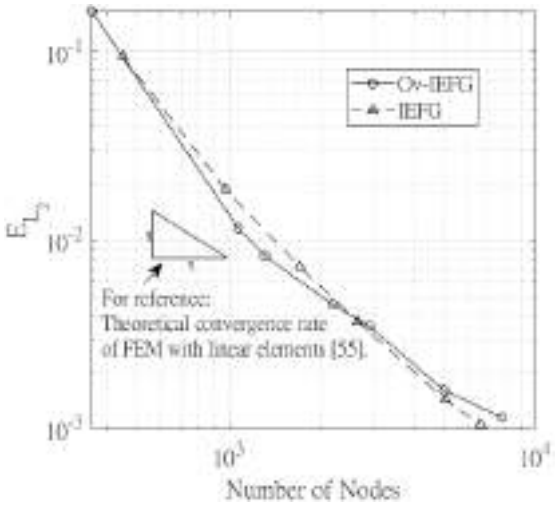

(a) t=5 s

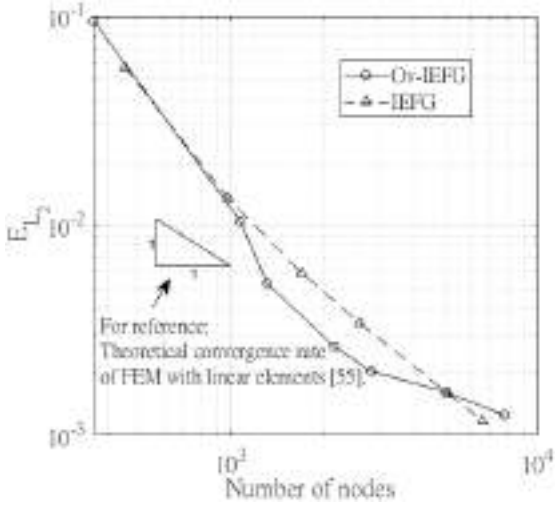

(b) t=25 s

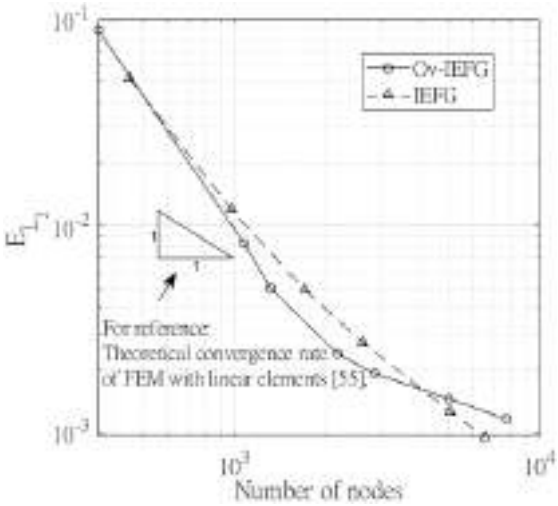

(c) t=50 s

Figure 22: Comparison of the convergence behaviour achieved via both the Ov-IEFG and standard IEFG techniques with respect to the highly refined FEM-based benchmark results, at times (a) t=5 s, (b) t=25 s, and (c) t=50 s.

Such procedures are cumbersome and particularly computing demanding within the framework of EFG methods, since also involve the need for finding the support domain nodes at each integration point according to the updated nodes distribution. The search for support domain nodes at each integration point is actually the most time-consuming calculation procedure in EFG methods, and several comprehensive discussions concerning the development of more efficient techniques for finding neighbouring nodes and constructing shape functions in EFG methods[61,62] and other meshless techniques[62,63] can be found in the literature. The solution of transient heat conduction problems with moving heat sources using dynamic nodes reconfiguration algorithms within the framework of EFG methods and related implementation aspects is beyond the scopes of this communication, which is actually focused on the achievement of accurate results via an easier-to-implement alternative Ov-IEFG approach.

It has already been mentioned that the proposed Ov-IEFG technique is an alternative approach particularly conceived to achieve enriched solutions of transient heat conduction problems with moving heat sources, without the need of performing the cumbersome and computing demanding procedures concerning the implementation of adaptive nodes refinement algorithms. The simple rigid body motion of the patch nodes used in the Ov-IEFG approach to follow the path of the moving heat source and properly capture the marked thermal gradients developed near it removes the need of performing at each time step the search for support domain nodes of each integration point, which is actually the most time consuming part of EFG methods. In this sense, it is also important to discuss the implications of such positive feature in the computing performance of the Ov-IEFG technique. Numerical solutions have been performed on a i7-7500U 2.90 GHz (i7 is a trademark of Intel Corporation, Santa Clara, C. A., USA) processor running the WINDOWS10 Home Basic (WINDOWS is a trademark of the Microsoft Corporation, Redmond, C. A. USA) operating system with 12 GB of RAM installed. The numerical procedures performed during the search for support domain nodes at each integration point, construction of IMLS approximations and assembly of matrices concerning the Ov-IEFG and standard IEFG techniques have taken 32.6 and 32.08 seconds, respectively. The computing times are referred to the finest nodes distributions used in the current accuracy analysis, which are depicted in Fig.21(a)-(b). Solving the system of equations at each time step has taken 0.36 seconds approximately under the Ov-IEFG approach, whereas it has taken only 0.1 seconds approximately under the standard IEFG method. This is related to the iterative procedure required at each time step in the Ov-IEFG approach, which is performed until convergence is reached in the CDC imposed to transfer information between the arrangements of background and patch nodes. According to these results, the standard IEFG approach exhibits a better computing performance in this particular benchmark case where the assumption of a fixed position for the moving heat source via the Rosenthal's coordinates transformation has been feasible due to the problem simplicity. Under such particular conditions, the computing demanding procedures concerning the search for support domain nodes at each integration point, construction of IMLS approximations and assembly of matrices are performed only once regardless of whether the Ov-IEFG approach or the standard IEFG method is used. The situation is completely different in the cases for which the proposed Ov-IEFG technique has been actually conceived, i.e. problems where following the moving heat source path is mandatory given that performing the Rosenthal's approximation would lead to unaccurate results. Solving problems of this kind via a standard IEFG approach subjected to an adaptive nodes refinement near the heat source involves noteworthy changes in the arrangement of nodes representing the problem domain during the transient heat conduction analysis, which would increase the computing time to more than 30 seconds between successive configurations of the transient problem. Such a significant increase in the computing time is related to the need of finding the neighbouring nodes at each integration point, constructing the IMLS approximations and reassembling the matrices at each time step, which are computing demanding procedures performed only once under a fixed nodes distribution. On the other hand, the requirement of performing such computing-time demanding numerical procedures has been circumvented in the problems addressed so far via the proposed Ov-IEFG technique. The configuration of both the background and patch nodes remains unchanged under this approach, whereas the fine arrangement of patch nodes merely perform a simple rigid body motion following the path of the moving heat source. As discussed so far, such a feature of the Ov-IEFG approach is the reason for which the information concerning the support domain nodes at each integration point and the IMLS approximations can be processed only once and kept throughout the entire transient heat conduction analysis. Although the time required to solve the system of equations at each time step under the Ov-IEFG approach is approximately 0.4 seconds due to the iterations performed to reach convergence in the CDC, it is substantially less than the 30 seconds or more that would be required in the computing-time demanding procedures involved in a standard IEFG method with adaptive nodes refinement. Such aspects demonstrate that the Ov-IEFG technique proposed in this communication significantly excels the computing performance of a standard IEFG formulation coupled to an adaptive nodes refinement procedure, in problems where the moving heat source location must be actually known at each time step.

4.3. Extension to three-dimensional problems with curved geometries and temperature dependent properties

The results discussed so far in this communication have been useful to demonstrate the feasibility and reliability of using the proposed Ov-IEFG technique to properly capturing the effect of highly concentrated moving heat sources in

transient conduction heat transfer problems, which is crucial to achieve an appropriate prediction of arc welding processes performance. Such aspect has been proven not only in the solution of a simple problem involving a moving heat source following a horizontal straight path in a rectangular geometry, but also in a more interesting situation involving a point heat source moving along a curve path in a non-rectangular geometry. However, such problems addressed so far are linear given that the thermal properties of the material have been considered to be constant. Additionally, the domain geometry in both cases does not have introduced significant complications in the numerical solution via the proposed Ov-IEFG technique. The actual potential of this novel approach will now be put into proper perspective via the solution of a three-dimensional problem with a more complex geometry, including also temperature-dependent material properties and phase change effects. Solving a problem of this kind is actually useful to demonstrate the possibility of using the Ov-IEFG technique in real applied situations where following the moving heat source path is mandatory, and simplified approaches (such as Rosenthal's) do not hold [8,10]. An outline of the problem to be solved is given in Fig.23, which is a circumferential arc-shaped part made of low-carbon structural steel S235JR. The heat input concerning the welding process is represented by a split or composite heat source model, which is also depicted in Fig.23. Such a composite heat source model comprises a surface part with an effective circular area and a truncated cone-shaped volumetric part, which are described by the following Gaussians distributions [8]:

$$\begin{aligned} \dot{Q}^S &= \dot{Q}_0^S e^{-r^2/r_o^2}, \qquad \text{Surface part,} \\ \dot{Q}^V &= \dot{Q}_0^V e^{-r^2/r_V(z)^2}, \qquad \text{Volumetric part,} \end{aligned} \tag{22}$$

where $\dot{Q}_0^S$ and $\dot{Q}_0^V$ are the maximum energy per unit area of the surface part and the maximum energy per unit volume of the volumetric part, respectively. Such values are computed as:

$$\dot{Q}_0^S = (1-\gamma)\frac{Q_T}{\pi r_0^2}, \qquad \dot{Q}_0^V = \gamma\frac{3Q_T}{(z_i - z_e)\pi(r_i^2 + r_e^2 + r_i r_e)}, \tag{23}$$

where Q_T is the total power of the composite heat source, whereas γ is the fraction of the power Q_T that is provided by the volumetric part [64]. The geometric parameters r_0, r_i, r_e, z_i and z_e involved in Eq.(23) are depicted appropriately in Fig.23. The parameter r in the composite heat source model is the distance from a given point to the symmetry axis of the moving heat source, and the cross-sectional radius of the truncated cone $r_V(z)$ varies linearly in the axial direction according to:

$$r_V(z) = r_i - \frac{r_i - r_e}{z_i - z_e}(z_i - z) \tag{24}$$

The heat source moves at the upper surface along the arc-shaped part mid-radius R, with a velocity of constant magnitude $||\vec{v}||$, whereby the current position of the heat source centre $\vec{x}_s(t)$ is given by:

$$\vec{x}_s(t) = \begin{cases} x_s(t) = R[1 - cos(\omega t)] \text{ (mm)}, \\ y_s(t) = R\, sin(\omega t) \text{ (mm)}, \\ z_s(t) = H \text{ (mm)} \end{cases} \qquad 0 \le t \le 40 \text{ (s)} \tag{25}$$

where $\omega = ||\vec{v}||/R$. Accordingly, the moving heat source velocity $\vec{v}(t) = (u_s(t), v_s(t), w_s(t))$ is given by:

$$\vec{v}(t) = \begin{cases} u_s(t) = ||\vec{v}||sin(\omega t) \text{ (mm/s)}, \\ v_s(t) = ||\vec{v}||cos(\omega t) \text{ (mm/s)}, \\ w_s(t) = 0 \text{ mm/s} \end{cases} \qquad 0 \le t \le 40 \text{ (s)} \tag{26}$$

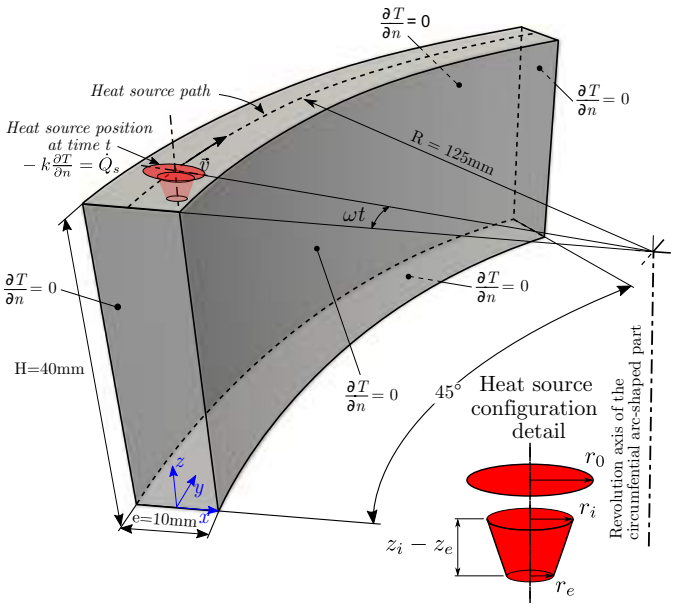

Figure 23: Configuration and boundary conditions of the three-dimensional problem with curved geometry and temperature-dependent material properties.

The material properties of the low-carbon structural steel S235JR, and the welding parameters are given in Tab.3. Additionally, the dimensions required to define the problem geometry have already been depicted appropriately in Fig.23. The dependence of material properties on temperature is given in terms of the volume fraction of solid phase $f_s(T)$ as follows:

$$\begin{aligned} k(T) &= k_s f_s(T) + k_l[1 - f_s(T)], \\ C_p(T) &= C_{ps} f_s(T) + C_{pl}[1 - f_s(T)], \\ \rho(T) &= \rho_s f_s(T) + \rho_l[1 - f_s(T)], \end{aligned} \tag{27}$$

with the solid fraction computed according to:

$$f_s(T) = \begin{cases} 1 & T < T_{sol}, \\ \frac{T_{liq} - T}{T_{liq} - T_{sol}} & T_{sol} \le T \le T_{liq}, \\ 0 & T > T_{liq}, \end{cases} \tag{28}$$

whereas the marked non-linearity concerning the solid-liquid phase change effects is included via the effective specific heat approach:

$$C_p^{eff}(T) = C_p(T) - H_f \frac{df_s}{dT} \tag{29}$$

Table 3: Welding parameters and material properties concerning the three-dimensional applied problem.

Welding parameters	Values
Initial temperature T_0 (K)	298
Total power of the composite heat source Q_T (W)	450
Fraction provided by the volumetric part γ	0.7
Effective radius of the surface part r_0 (mm)	0.8
Upper radius of the truncated cone r_i (mm)	0.6
Lower radius of the truncated cone r_e (mm)	0.3
Axial position of the upper radius z_i (mm)	39.8
Axial position of the lower radius z_e (mm)	35.8
Velocity magnitude of the moving heat source $\|\|\vec{v}\|\|$ (mm/s)	2
Material properties [65]	Values
Conductivity of solid phase k_s (W.mm^{-1}.K^{-1})	0.045
Conductivity of liquid phase k_l (W.mm^{-1}.K^{-1})	0.090
Specific heat capacity of solid phase C_{ps} (J.kg^{-1}.K^{-1})	480
Specific heat capacity of liquid phase C_{pl} (J.kg^{-1}.K^{-1})	480
Density of solid phase ρ_s (kg.mm^{-3})	7.6×10^{-6}
Density of liquid phase ρ_l (kg.mm^{-3})	7.6×10^{-6}
Fusion latent heat H_f (J.kg^{-3})	256000
Solidus temperature T_{sol} (K)	1739.8
Liquidus temperature T_{liq} (K)	1790.1

The transient problem has been solved under a fully implicit backward finite difference scheme with a time step of $\Delta t = 0.5$ s, and now the iterative process is performed until convergence is reached in both the CDC and non-linearities concerning the temperature-dependent properties and phase change effects. The arrangement of overlapping nodes at different times are depicted in Fig.24(a)-(c), where the patch nodes perform a purely rotational rigid body motion around the revolution axis of the arc-shaped part. The rigid body motion is such that the symmetry axis of the moving heat source remains in the centre of the patch nodes arrangement during the entire transient heat conduction analysis, i.e. the patch nodes move with angular velocity $\omega = ||\vec{v}||/R$. The background arrangement consists of 22869 nodes, whereas 15129 nodes are included in the fine patch arrangement. The temperature distributions corresponding to the configurations depicted in Fig.24(a)-(c) are given in Fig.25(a)-(c) and Fig.26. Fig.25(a)-(c) depicts the temperature at the domain outer surface, whereas the temperature distribution in axial slices located at the heat source position at each time step are given in Fig.26. The Ov-IEFG approach has allowed the appropriate capture of the high temperatures and marked thermal gradients developed near the moving heat source also in the current three-dimensional problem, which also includes non-linearities related to the temperature-dependent material properties. The smooth and stable temperature distributions both on the outer surface and within the domain demonstrate both the convergence on the non-linear aspects and the appropriate transfer of information achieved though the immersed boundaries $\Gamma_{\mathrm{BG}\to\mathrm{PC}}$ and $\Gamma_{\mathrm{PC}\to\mathrm{BG}}$, whose details are depicted in Fig.27 for visualization purposes. The achievement of such smooth and stable results under the solid-liquid phase change effects has provided a robust validation of the Ov-IEFG technique potential in the thermal modelling of welding, since the heat released during such transition introduces one of the more complex material non-linearities to be solved in order to predict the performance of these processes under real conditions [9,65,66]. The solution obtained via the Ov-IEFG approach has been compared to a standard FEM-based solution with the mesh depicted in Fig.28, which has had to be highly refined and clustered towards the domain upper-surface to capture appropriately the moving heat source effects. Such a mesh consists of 627200 elements and 660633 nodes, which significantly exceeds (by a factor of more than 17) the 22869+15129=37998 nodes used under the Ov-IEFG technique. The temperature profiles computed under both the Ov-IEFG technique and the FEM along the arc length s covered by the moving heat source path are compared in Fig.29, and the results obtained exhibit an excellent agreement between both numerical solutions at different times. Despite the greater complexity of the current problem, the temperature profiles computed under the Ov-IEFG still exhibits a continuous and smooth transition in the region of coupling between both arrangements of nodes. It is worth to mention that although the rigid motion of the patch nodes arrangement still allows the possibility of keeping the same support domain nodes at each integration point in Ω_{PC} during the entire transient analysis, the change of orientation that such arrangement undergoes in this case due to the rotation around the revolution axis of the domain geometry leads to the need of constructing the IMLS approximations at each time step.

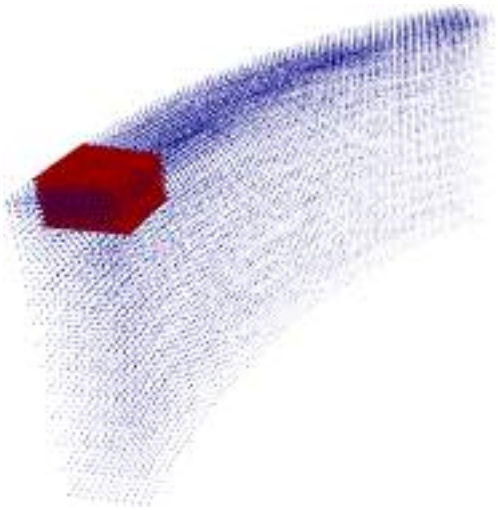

(a) t=5 s

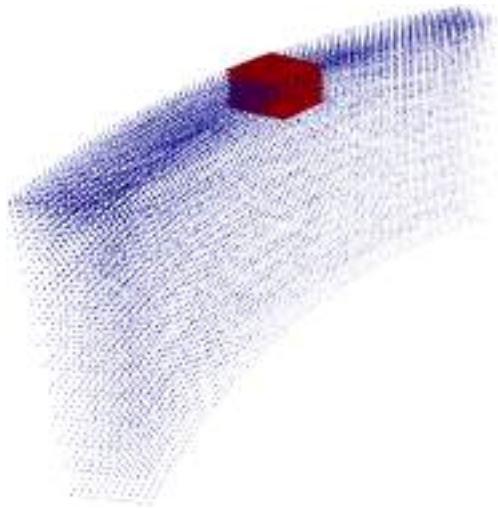

(b) t=25 s

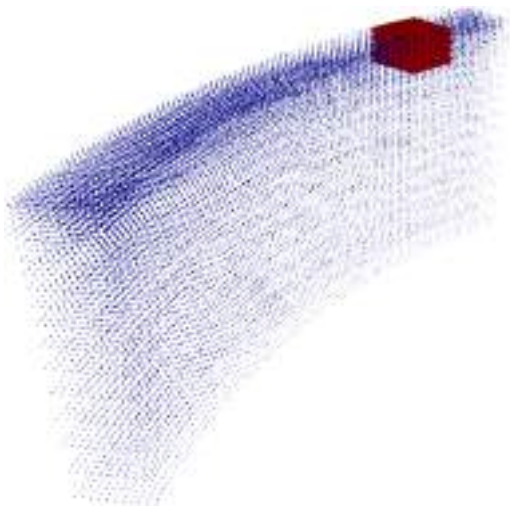

(c) t=40 s

Figure 24: Overlapping nodes arrangement used in the solution of the three-dimensional problem with curved geometry and temperature-dependent material properties. The background and patch nodes are depicted in blue and red, respectively.

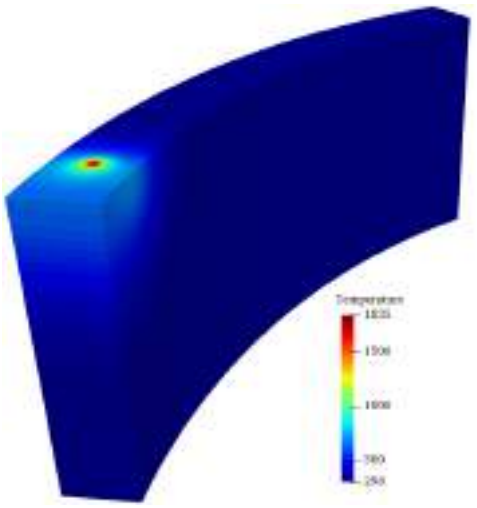

(a) t=5 s

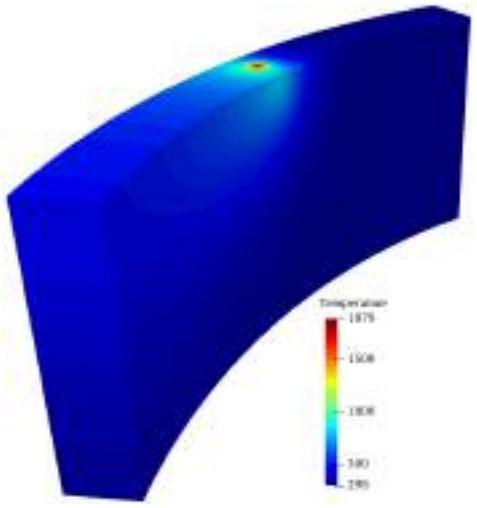

(b) t=25 s

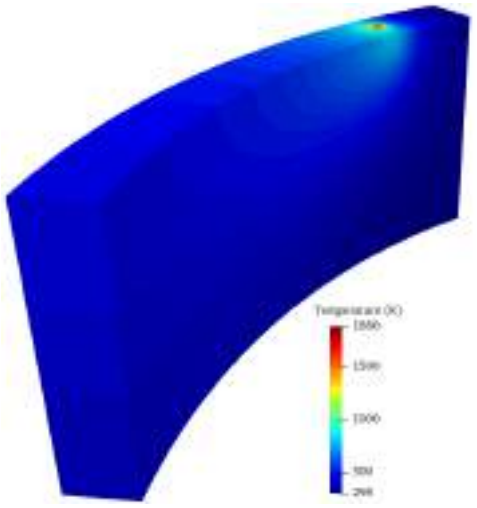

(c) t=40 s

Figure 25: Outer surface temperatures computed via the proposed Ov-IEFG technique, for the three-dimensional problem with curved geometry and temperature-dependent properties.

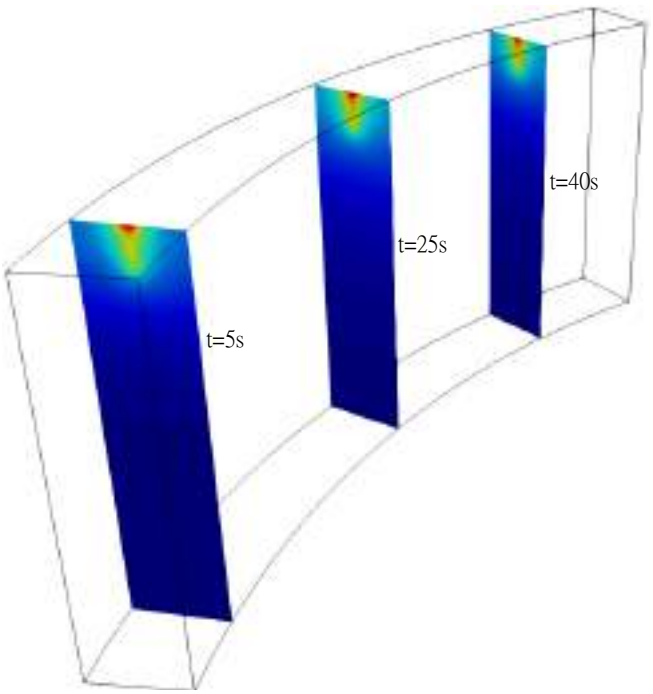

Figure 26: Temperature distributions in axial slices located at the position occupied by the moving heat source at diffent times.

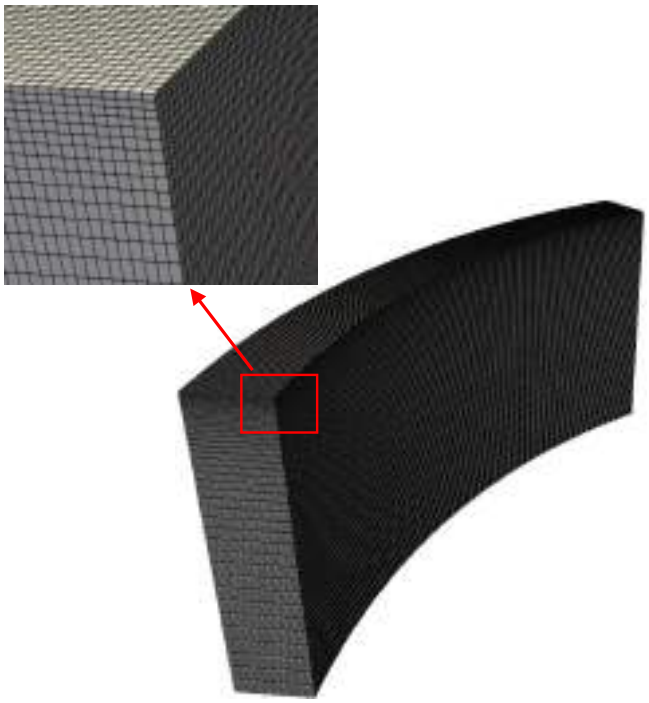

Figure 28: Mesh used in the standard FEM-based solution of the three-dimensional problem with curved geometry and temperature dependent material properties

Additionally, the matrices must also be assembled at each time step due to the non-linearities introduced by the temperature-dependent material properties and phase change effects. However, the Ov-IEFG technique continues to save significant computing time under such conditions, since -as discussed so far- the searching for support domain nodes at each integration point is the most computing demanding procedure in the numerical implementation of EFG methods.

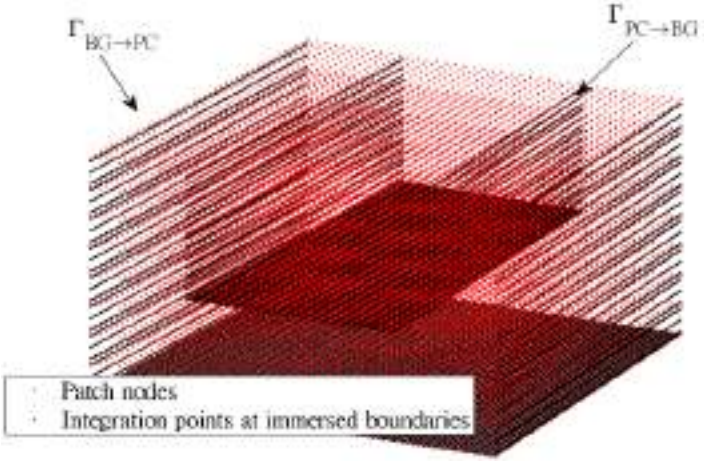

Figure 27: Detail of the immersed boundaries moving with the patch nodes arrangement for the transfer of information between the overlapping domains Ω_{BG} and Ω_{PC}, during the solution of the three-dimensional problem with curved geometry and temperature dependent material properties

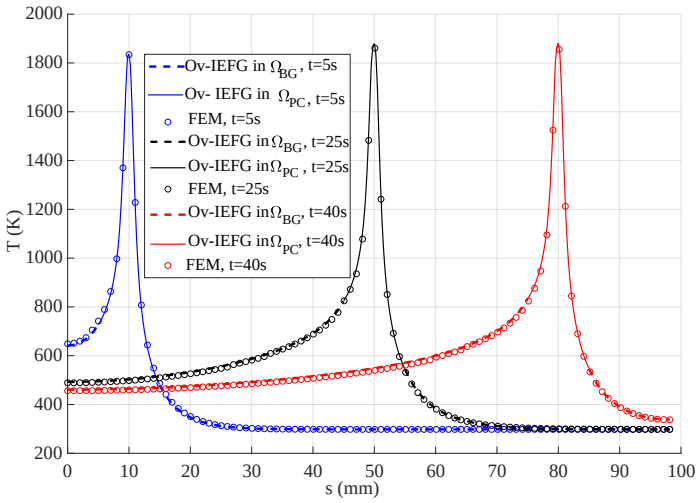

Figure 29: Comparison of the temperature profile computed via the Ov-IEFG technique along the arc length s covered by the moving heat source, with those obtained from a standard FEM-based solution.

Actually, the remarkably low number of nodes required to solve this problem via the Ov-IEFG technique has given rise to computing times shorter than those required in the FEM-based solution. Solving the non-linear thermal problem between successive time steps under the Ov-IEFG approach has taken approximately 450 seconds, whereas it has taken about 900 seconds under the FEM. This is not easy

to achieve in EFG methods, whose computational requirements would significantly exceed those of standard mesh-based approaches if implemented with the same number of nodes[14]. This is actually the main idea of recent work devoted to explore new possibilities in the formulation of EFG methods[67–69], i.e. proposing alternative approaches which are easy to implement in the context of this numerical techniques in order to reduce number of nodes required and saving computing time.

5. Conclusions

In this communication, a novel overlapping nodes scheme based on the improved element-free Galerkin method has been developed and successfully implemented in the solution of transient heat conduction problems with moving heat sources inherent in arc welding processes. Such an overset improved element-free Galerkin approach uses a fine arrangement of patch nodes undergoing a rigid body motion over a coarse arrangement of fixed nodes, according to the path followed by the moving heat source. The patch nodes have allowed an accurate computation of both temperature distributions and conductive heat flux in the moving heat source vicinity, whose effects could not be properly captured by the coarse arrangement of fixed nodes. The smoothness and continuity features of the improved moving least squares approximations have allowed a straightforward transfer of information between the overlapping arrangements of patch and background nodes, performing a continuous imposition of coupling Dirichlet conditions via the penalty method. There has been no need for complex post-processing or local reconstruction techniques to achieve a smooth and continuous coupling between both the temperature distributions and conductive heat fluxes computed over each nodes arrangement, which is a feature that excels the overset techniques developed so far in the context of both finite element and finite volume methods. The proposed overset improved element-free Galerkin method allows the achievement of very accurate and smooth solutions in transient heat conduction problems inherent in arc welding processes, regardless both the effective area and path of the heat source. An accuracy analysis performed within the framework of a simple benchmark problem formulated under the Rosenthal's approach has demonstrated the convergence behaviour of the proposed technique, which exhibited an accuracy similar to a standard improved element-free Galerkin-based solution performed under a single nodes distribution clustered near the moving heat source. It has also been demonstrated the better computing performance of the overset improved element-free Galerkin technique in the context of problems where it is mandatory to follow the moving heat source path, compared to that which would be achieved via a conventional improved element-free Galerkin-based solution performed under an adaptive nodes refinement procedure. The rigid body motion performed by the fine distribution of patch nodes has been useful to overcome the need of defining the nodal influence domains, conforming the integration points, and searching for the support domain nodes at each integration point between successive nodes configurations, which are cumbersome and computing demanding procedures required in meshless solutions performed under adaptive nodes refinement techniques. The positive features of the technique proposed in this communication have also been successfully extended to the solution of a three-dimensional problem involving a more complex geometry and marked non-linearities concerning the material properties, which has been useful to demonstrate the actual potential of this novel approach to predict the thermal performance of welding processes in real conditions. In summary, this novel approach provides a more comprehensive and efficient use of the positive features concerning the improved-element free Galerkin method in order to solve heat transfer problems in arc welding processes subjected to more complex conditions than those affordable in the context of standard fixed nodes meshless solutions.

References

[1] Nhan T. Nguyen, Akihiko Ohta, Kazuyoshi Matsuoka, Naoyuki Suzuki, and Yoshio Maeda. Analytical solutions for transient temperature of semi-infinite body subjected to 3-D moving heat sources. *Welding Journal*, 78:265–274, 1999.

[2] Nhan T. Nguyen, Yiu-Wing Mai, S. Simpson, and Akihiko Ohta. Analytical Approximate Solution For Double Ellipsoidal Heat Source In Finite Thick Plate. *Welding Journal*, 83(82–93), 2004.

[3] Jerzy Winczek. Analytical solution to transient temperature field in a half-infinite body caused by moving volumetric heat source. *International Journal of Heat and Mass Transfer*, 53(25-26):5774–5781, 2010.

[4] Víctor D. Fachinotti, Andrés Amílcar Anca, and Alberto Cardona. Analytical solutions of the thermal field induced by moving double-ellipsoidal and double-elliptical heat sources in a semi-infinite body. *International Journal for Numerical Methods in Biomedical Engineering*, 27(4):595–607, 2011.

[5] D. W. M. Veldman, R. H. B. Fey, H. J. Zwart, M. M. J. van de Wal, J. D. B. J. van den Boom, and H. Nijmeijer. Semi-analytic approximation of the temperature field resulting from moving heat loads. *International Journal of Heat and Mass Transfer*, 122:128–137, 2018.

[6] T. F. Flint, J. A. Francis, M. C. Smith, and A. N. Vasileiou. Semi-analytical solutions for the transient temperature fields induced by a moving heat source in an orthogonal domain. *International Journal of Thermal Sciences*, 123:140–150, 2018.

[7] Xuan-Tan Pham. Two-Dimensional Rosenthal Moving Heat Source Analysis Using the Meshless Element Free Galerkin Method. *Numerical Heat Trasnfer, Part A: Applications*, 63(11):807–823, jun 2013.

[8] Olivier Champagne and Xuan-Tan Pham. Numerical simulation of moving heat source in arc welding using the Element-free Galerkin method with experimental validation and numerical study. *International Journal of Heat and Mass Transfer*, 154:119633, 2020.

[9] Andrés Anca, Alberto Cardona, José Risso, and Víctor D. Fachinotti. Finite element modeling of welding processes. *Applied Mathematical Modelling*, 35(2):688–707, 2011.

[10] Songtao Chen and Qinglin Duan. An adaptive second-order element-free Galerkin method for additive manufacturing process. *Computational Materials Science*, 183:109911, 2020.

[11] Fatemeh Hejripour, Brian T. Helenbrook, Daniel T. Valentine, and Daryush K. Aidun. Mass transport and solidification phenomenon in dissimilar metals arc welding. *International Journal of Heat and Mass Transfer*, 144:118703, 2019.

[12] Zhicheng Hu and Zhihui Liu. Heat Conduction Simulation of 2D Moving Heat Source Problems Using a Moving Mesh Method. *Advances in Mathematical Physics*, 2020:1–16, 2020.

[13] Kajal Khan, Gunther Mohr, Kai Hilgenberg, and A. De. Probing a novel heat source model and adaptive remeshing technique to simulate laser powder bed fusion with experimental validation. *Computational Materials Science*, 181:109752, 2020.

[14] G. R. Liu. *Mesh Free Methods*. CRC Press, second edition, 2009.

[15] Xiaohua Zhang and Hui Xiang. A fast meshless method based on proper orthogonal decomposition for the transient heat conduction problems. *International Journal of Heat and Mass Transfer*, 84:729–739, 2015.

[16] Edgar O. Reséndiz-Flores and Irma D. García-Calvillo. Numerical solution of 3D non-stationary heat conduction problems using the Finite Pointset Method. *International Journal of Heat an Mass Transfer*, 87:104–110, 2015.

[17] Jianping Zhang, Guoqiang Zhou, Shuguang Gong, and Shusen Wang. Transient heat transfer analysis of anisotropic material by using Element-Free Galerkin method. *International Communications in Heat and Mass Transfer*, 84:134–143, may 2017.

[18] Jianping Zhang, Yang Shen, Huiyao Hu, Shuguang Gong, Shuying Wu, Zhiqi Wang, and Jian Huang. Transient heat transfer analysis of orthotropic materials considering phase change process based on element-free Galerkin method. *International Communications in Heat and Mass Transfer*, 125:105295, 2021.

[19] Yan Gu, Lei Wang, Wen Chen, Chuanzeng Zhang, and Xiaoqiao He. Application of the meshless generalized finite difference method to inverse heat source problems. *International Journal of Heat and Mass Transfer*, 108:721–729, 2017.

[20] Cheng-Yu Ku, Chih-Yu Liu, Weichung Yeih, Chein-Shan Liu, and Chia-Ming Fan. A novel space–time meshless method for solving the backward heat conduction problem. *International Journal of Heat and Mass Transfer*, 130:109–122, 2019.

[21] Ping Zhang, Xiaohua Zhang, Jiheng Deng, and Laizhong Song. A numerical study of natural convection in an inclined square enclosure with an elliptic cylinder using variational multiscale element free Galerkin method. *International Journal of Heat and Mass Transfer*, 99:721–737, aug 2016.

[22] Yu Yang and Sy-bor Wen. A new high accuracy meshfree method to directly simulate fluid dynamics and heat transfer of weakly compressible fluids. *International Journal of Heat and Mass Transfer*, 123:25–39, 2018.

[23] Edgar O. Reséndiz-Flores and Félix R. Saucedo-Zendejo. Numerical simulation of coupled fluid flow and heat transfer with phase change using the Finite Pointset Method. *International Journal of Thermal Sciences*, 133:13–21, 2018.

[24] Edgar O. Reséndiz-Flores and Félix R. Saucedo-Zendejo. Meshfree numerical simulation of free surface thermal flows in mould filling processes using the Finite Pointset Method. *International Journal of Thermal Sciences*, 127:29–40, may 2018.

[25] Mohammad Ali Iranmanesh and Ali Pak. Extrinsically enriched element free Galerkin method for heat and fluid flow in deformable porous media involving weak and strong discontinuities. *Computers and Geotechnics*, 103:179–192, 2018.

[26] J. C. Álvarez-Hostos, A. D. Bencomo, E. S. Puchi Cabrera, and I. M. Figueroa Poleo. A pseudo-transient heat transfer simulation of a continuous casting process, employing the element-free Galerkin method. *International Journal of Cast Metals Research*, 31(1):47–55, 2017.

[27] Juan C. Álvarez-Hostos, Alfonso D. Bencomo, Eli S. Puchi-Cabrera, Víctor D. Fachinotti, Benjamín Tourn, and Joselynne C. Salazar-Bove. Implementation of a standard stream-upwind stabilization scheme in the element-free Galerkin based solution of advection-dominated heat transfer problems during solidification in direct chill casting processes. *Engineering Analysis with Boundary Elements*, 106:170–181, sep 2019.

[28] J. C. Álvarez-Hostos, A. D. Bencomo, and E. S. Puchi Cabrera. Element-free Galerkin formulation for solving transient heat transfer problems of direct chill casting processes. *Canadian Metallurgical Quarterly*, 56(2):156–167, 2017.

[29] Juan C. Álvarez-Hostos, Erick A. Gutierrez-Zambrano, Joselynne C. Salazar Bove, Eli S. Puchi-Cabrera, and Alfonso D. Bencomo. Solving heat conduction problems with phase-change under the heat source term approach and the element-free Galerkin formulation. *International Communications in Heat and Mass Transfer*, 2019.

[30] Yi-Bin Hong and Chih-Yang Wu. Integral equation solutions using radial basis functions for radiative heat transfer in higher-dimensional refractive media. *International Journal of Heat and Mass Transfer*, 118:1180–1189, 2018.

[31] Jie Sun, Hong-Liang Yi, Ming Xie, and He-Ping Tan. New implementation of local RBF meshless scheme for radiative heat transfer in participating media. *International Journal of Heat and Mass Transfer*, 95:440–452, apr 2016.

[32] Qiyin Lin, Jihong Wang, Jun Hong, Zheng Liu, and Zhihua Wang. A biomimetic generative optimization design for conductive heat transfer based on element-free Galerkin method. *International Communications in Heat and Mass Transfer*, 100:67–72, 2019.

[33] Edgar O. Reséndiz-Flores and Félix R. Saucedo-Zendejo. Two-dimensional numerical simulation of heat transfer with moving heat source in welding using the Finite Pointset Method. *International Journal of Heat and Mass Transfer*, 90:239–245, 2015.

[34] A. Khosravifard, M. R. Hematiyan, and N. Ghiasi. A meshfree method with dynamic node reconfiguration for analysis of thermo-elastic problems with moving concentrated heat sources. *Applied Mathematical Modelling*, 79:624–638, 2020.

[35] Yihua Xiao, Haifei Zhan, Yuantong Gu, and Qinghua Li. Modeling heat transfer during friction stir welding using a meshless particle method. *International Journal of Heat and Mass Transfer*, 104:288–300, 2017.

[36] Ali Moarrefzadeh, Shahram Shahrooi, and Mahdi Jalali Azizpour. The application of the meshless local Petrov-Galerkin method for the analysis of heat conduction and residual stress due to welding. *The International Journal of Advanced Manufacturing Technology*, 104(1-4):723–742, 2019.

[37] G. G. Stubblefield, K. Fraser, B. J. Phillips, J. B. Jordon, and P. G. Allison. A meshfree computational framework for the numerical simulation of the solid-state additive manufacturing process, additive friction stir-deposition (AFS-D). *Materials and Design*, 202:109514, 2021.

[38] Juan C. Álvarez-Hostos, Eli S. Puchi-Cabrera, and Alfonso D. Bencomo. Stress Analysis of a Continuous Casting Process, on the Basis of the Element-Free Galerkin Formulation. *steel research international*, 88(2):1600019, 2016.

[39] Juan Carlos Álvarez-Hostos, A. D. Bencomo, and E. S. Puchi Cabrera. Simple iterative procedure for the thermal-mechanical analysis of continuous casting processes, using the element-free Galerkin method. *Journal of Thermal Stresses*, 41(2):160–181, 2018.

[40] J. C. Álvarez-Hostos, A. D. Bencomo, E. S. Puchi Cabrera, J.-D. Guérin, and L. Dubar. Modeling the viscoplastic flow behavior of a 20MnCr5 steel grade deformed under hot-working conditions, employing a meshless technique. *International Journal of Plasticity*, 103:119–142, 2018.

[41] Juan C. Álvarez-Hostos, Victor D. Fachinotti, Alirio J. Sarache Piña, Alfonso D. Bencomo, and Eli S. Puchi-Cabrera. Implementation of standard penalty procedures for the solution of incompressible Navier-Stokes equations, employing the element-free Galerkin method. *Engineering Analysis with Boundary Elements*, 96:36–54, 2018.

[42] Juan C. Álvarez-Hostos, Joselynne C. Salazar-Bove, Marcela A. Cruchaga, Víctor D. Fachinotti, and Rafael A. Mujica-Agelvis. Solving steady-state lid-driven square cavity flows at high Reynolds numbers via a coupled improved element-free Galerkin–reduced integration penalty method. *Computers and Mathematics with Applications*, 99:211–228, 2021.

[43] Juan C. Álvarez-Hostos, Marcela A. Cruchaga, Víctor D. Fachinotti, Javier A. Zambrano Carrillo, and Esteban Zamora. A plausible extension of standard penalty, streamline upwind and immersed boundary techniques to the improved element-free Galerkin-based solution of incompressible Navier–Stokes equations. *Computer Methods in Applied Mechanics and Engineering*, 372:113380, 2020.

[44] Jianghong Chen, Xiaohua Zhang, Ping Zhang, and Jiheng Deng. Variational multiscale element free Galerkin method for natural convection with porous medium flow problems. *International Journal of Heat and Mass Transfer*, 107:1014–1027, 2017.

[45] Mehdi Dehghan and Niusha Narimani. An element-free Galerkin meshless method for simulating the behavior of cancer cell invasion of surrounding tissue. *Applied Mathematical Modelling*, 59:500–513, 2018.

[46] Mehdi Dehghan and Niusha Narimani. The element-free Galerkin method based on moving least squares and moving Kriging approximations for solving two-dimensional tumor-induced angiogenesis model. *Engineering with Computers*, 2019.

[47] G. Karami and M. R. Hematiyan. A boundary element method of inverse non-linear heat conduction analysis with point and line heat sources. *Communications in Numerical Methods in Engineering*, 16(3):191–203, 2000.

[48] Frédéric Lefèvre and Christophe Le Niliot. The BEM for point heat source estimation: application to multiple static sources and moving sources. *International Journal of Thermal Sciences*, 41(6):536–545, 2002.

[49] M. R. Hematiyan, M. Mohammadi, and M. H. Aliabadi. Boundary element analysis of two- and three-dimensional thermo-elastic problems with various concentrated heat sources Boundary element analysis of two- and three-dimensional thermo-elastic problems with various concentrated heat sources. *The Journal of Strain Analysis for Engineering Design*, 46(3):227–242, 2011.

[50] M. Mohammadi, M. R. Hematiyan, and A. Khosravifard. Boundary element analysis of 2D and 3D thermoelastic problems containing curved line heat sources. *European Journal of Computational Mechanics*, 25(1-2):147–164, 2016.

[51] M. Mohammadi, M. R. Hematiyan, and A. Khosravifard. Analysis of Two- and Three-dimensional Steady-state Thermo-mechanical Problems Including Curved Line/Surface Heat SourcesUsing the Method of Fundamental Solutions. *European Journal of Computational Mechanics*, 28(1):51–80, 2019.

[52] Mehrdad Mohammadi. The Method of Fundamental Solutions for Two- and Three-Dimensional Transient Heat Conduction Problems Involving Point and Curved Line Heat Sources. *Iranian Journal of Science and Technology, Transactions of Mechanical Engineering*, 45(4):993–1005, 2019.

[53] M. Mohammadi, M. R. Hematiyan, and Y. C. Shiah. An efficient boundary-type meshfree method for analysis of two-dimensional laser heating problems. *Engineering Analysis with Boundary Elements*, 132:460–468, 2021.

[54] M. Mohammadi and M. R. Hematiyan. Analysis of transient uncoupled thermoelastic problems involving moving point heat sources using the method of fundamental solutions. *Engineering Analysis with Boundary Elements*, 123:122–132, 2021.

[55] Bruno Storti, Luciano Garelli, Mario Storti, and Jorge D'Elía. A matrix-free Chimera approach based on Dirichlet–Dirichlet coupling for domain composition purposes. *Computers and Mathematics with Applications*, 79(12):3310–3330, 2020.

[56] Jean Donea, Antonio Huerta, Jean-Philippe Ponthot, and Antonio Rodríguez-Ferran. Arbitrary Lagrangian-Eulerian Methods, 2017.

[57] D. Rosenthal. The Theory of Moving Sources of Heat and Its Application to Metal Treatments. *Transactions Asme*, (43):849–866, 1946.

[58] Peng Ding. Solution of lid-driven cavity problems with an improved SIMPLE algorithm at high Reynolds numbers. *International Journal of Heat and Mass Transfer*, 115:942–954, dec 2017.

[59] J. D. Jaeger. Moving Sources of Heat and the Temperature of Sliding Contacts. In *Proceedings of the Royal Society of New South Wales*, 1942.

[60] Xiaolin Li and Shuling Li. On the stability of the moving least squares approximation and the element-free Galerkin method. *Computers & Mathematics with Applications*, 72(6):1515–1531, 2016.

[61] S. H. Ju and H. H. Hsu. Solving numerical difficulties for element-free Galerkin analyses. *Computational Mechanics*, 53(2):273–281, 2013.

[62] James Olliff, Brad Alford, and Daniel C. Simkins. Efficient searching in meshfree methods. *Computational Mechanics*, 62(6):1461–1483, 2018.

[63] C. A. D. Fraga Filho, L. L. Schuina, and B. S. Porto. An Investigation into Neighbouring Search Techniques in Meshfree Particle Methods: An Evaluation of the Neighbour Lists and the Direct Search. *Archives of Computational Methods in Engineering*, 27(4):1093–1107, 2019.

[64] Yi Luo, Guoqiang You, Hong Ye, and Jinhe Liu. Simulation on welding thermal effect of AZ61 magnesium alloy based on three-dimensional modeling of vacuum electron beam welding heat source. *Vacuum*, 84(7):890–895, 2010.

[65] Hubert Danielewski and Andrzej Skrzypczyk. Steel Sheets Laser Lap Joint Welding—Process Analysis. *Materials*, 13(10):2258, 2020.

[66] Lei Wang, He Li, Yong Huang, Kehong Wang, and Ming Zhou. Effect of Preheating on Martensitic Transformation in the Laser Beam Welded AH36 Steel Joint: A Numerical Study. *Metals*, 12(1):127, 2022.

[67] Z. J. Meng, H. Cheng, L. D. Ma, and Y. M. Cheng. The hybrid element-free Galerkin method for three-dimensional wave propagation problems. *International Journal for Numerical Methods in Engineering*, 117(1):15–37, 2018.

[68] H. Cheng, M. J. Peng, and Y. M. Cheng. The dimension splitting and improved complex variable element-free Galerkin method for 3-dimensional transient heat conduction problems. *International Journal for Numerical Methods in Engineering*, 114(3):321–345, feb 2018.

[69] Jufeng Wang and Fengxin Sun. A hybrid generalized interpolated element-free Galerkin method for Stokes problems. *Engineering Analysis with Boundary Elements*, 111:88–100, 2020.